U–Pb geochronology of deformation and metamorphism across a central transect of the Early Proterozoic Torngat Orogen, North River map area, Labrador[1]

JEAN-MICHEL BERTRAND
Centre de recherches pétrographiques et géochimiques, B.P. 20, 54501 Vandoeuvre-lès-Nancy Cédex, France

J. CHRISTOPHER RODDICK
Geological Survey of Canada, 601 Booth Street, Ottawa, ON K1A 0E8, Canada

MARTIN J. VAN KRANENDONK[2]
Department of Geological Sciences, Queen's University, Kingston, ON K7L 3N6, Canada

AND

INGO ERMANOVICS
Geological Survey of Canada, 601 Booth Street, Ottawa, ON K1A 0E8, Canada

Received July 15, 1992
Revision accepted April 29, 1993

The Early Proterozoic Torngat Orogen resulted from the oblique collision of the Archean Nain and southeastern Rae provinces and evolved in four stages: (0) deposition of platformal supracrustal assemblages followed by subduction-related arc magmatism in the margin of the Rae Province; (I) crustal thickening and nappe tectonics; (II) sinistral transpression and formation of the Abloviak shear zone; (III) uplift on steeply dipping, east-verging mylonites along the eastern orogenic front.

U–Pb geochronology on zircon and monazite from major rock units and syntectonic intrusions indicates that arc magmatism at ca. 1880 Ma was followed by 40 Ma. of deformation and high-grade metamorphism from ca. 1860 to 1820. Subsequent uplift and final cooling occurred ca. 1795–1770 Ma. Several ages of mineral growth that correspond to distinct structural and metamorphic events have been recognized: (1) 1858–1853 Ma zircon and monazite dates are interpreted as the minimum age of stage I and peak metamorphic conditions; (2) 1844 Ma zircons from anatectic granitoids in the Tasiuyak gneiss complex (TGC), syntectonic with stage II deformation, are interpreted to date the formation of the Abloviak shear zone; (3) 1837 Ma magmatic zircons from an intrusive granite vein deformed along the western contact of the TGC represent a discrete intrusive event; (4) 1825–1822 Ma metamorphic overgrowths and newly grown zircons in granitic veins from the western portion of the orogen (Lac Lomier complex) represent a period of renewed transpressional deformation; (5) 1806 Ma magmatic zircons from a post-stage II granite emplaced along the eastern edge of the Abloviak shear zone defines the transition between stage II and stage III events; (6) 1794–1773 Ma zircons from leucogranites and pegmatites that are associated with uplift of the orogen (stage III). 1780–1740 Ma dates for monazite and a $^{40}Ar/^{39}Ar$ hornblende age correspond to the latest stages of uplift and cooling of the orogen.

L'orogène de Torngat, d'âge protérozoïque précoce, est le résultat de la collision oblique des provinces archéennes de Nain et du sud-est de Rae, et dont l'évolution passe par quatre stades: (0) le dépôt des assemblages supracrustaux de plate-forme suivi du magmatisme d'arc associé à la subduction dans la marge de la province de Rae; (I) un épaississement crustal et une tectonique de nappes; (II) une transpression senestre et développement de la zone de cisaillement d'Abloviak; (III) le soulèvement sur des mylonites de fort pendage et de vergence est, le long du front orogénique oriental.

La datation U–Pb sur zircon et monazite des principales unités lithologiques et des intrusions syntectoniques révèle que le magmatisme d'arc, il y a environ 1880 Ma, fut suivi par une période de déformation et de métamorphisme de degré élevé qui a duré 40 Ma, de 1860 à 1820 Ma, approximativement. Un soulèvement subséquent qui fut accompagné d'un refroidissement terminal s'est produit il y a environ 1795–1770 Ma. Il a été reconnu que plusieurs de ces âges de croissance des minéraux correspondaient à des événements structuraux et métamorphiques distincts, ce sont : (1) les âges 1858–1853 Ma sur zircon et monazite qui sont interprétés comme représentant un âge minimum du stade I et des conditions métamorphiques culminantes; (2) l'âge 1844 Ma sur zircons extraits des granitoïdes anatectiques du Complexe gneissique de Tasiuyak, syntectoniques de la déformation du stade II, est interprété comme l'âge de la formation de la zone de cisaillement d'Abloviak; (3) l'âge 1837 Ma sur les zircons magmatiques provenant d'un filon de granite intrusif, déformé le long du contact ouest du Complexe gneissique de Tasiuyak, représente un événement intrusif isolé; (4) l'âge 1825–1822 Ma sur les accroissements secondaires métamorphiques et les zircons de néocristallisation dans les filons granitiques de la région occidentale de l'orogène (Complexe du lac Lomier) représente une période de déformation transpressive réactivée; (5) l'âge de 1806 Ma fourni par les zircons magmatiques du granite postérieur au stade II, mis en place le long de la limite orientale de la zone de cisaillement d'Abloviak, définit la transition entre les événements des stades II et III; (6) les âges de 1794–1773 Ma obtenus pour les zircons provenant des leucogranites et des pegmatites sont liés au soulèvement de l'orogène (stade III). Les dates de 1780–1740 fournies par la monazite et un âge $^{40}Ar/^{39}Ar$ sur hornblende correspondent aux stades terminaux du soulèvement et du refroidissement de l'orogène.

[Traduit par la rédaction]

Can. J. Earth Sci. **30**, 1470–1489 (1993)

[1]Geological Survey of Canada Contribution 14393.
[2]Present address: Geological Survey of Canada, 601 Booth Street, Ottawa, ON K1A 0E8, Canada.

Printed in Canada / Imprimé au Canada

Introduction

The Early Proterozoic Torngat Orogen is a north–south to 160° striking belt of high-grade, strongly deformed rocks in the eastern part of the Laurentian Shield (Fig. 1), which resulted from transpressional collision between the Archean Nain Province and the southeastern arm of the Rae Province (former Churchill Province of Taylor 1979; Hoffman 1988; Wardle et al. 1990; Van Kranendonk and Ermanovics 1990). The Torngat Orogen is one of several interconnected orogenic belts of Early Proterozoic age (ca. 1.8 Ga; the Trans-Hudson Orogen, see Hoffman 1988) in the Laurentian Shield that record the amalgamation of Laurentia from a number of smaller Archean cratonic nuclei (Hoffman 1988). In this regard, knowledge of the exact timing of events in the Torngat and other orogenic belts is critical to our understanding of the tectonic evolution of northeastern Laurentia (e.g., Hoffman 1990; Van Kranendonk 1992*a*).

Previous workers established the major structural and metamorphic events in the evolution of the Torngat Orogen (Wardle 1983; Mengel and Rivers 1989, 1991; Mengel et al. 1991; Wardle et al. 1990), but did not correlate the sequence of these events across the width of the orogen or develop a fully integrated tectonic model owing to an absence of accurate geochronology and complete mapping. In this paper, we document the timing of magmatic and deformational events in the formation of the Torngat Orogen in the North River map area, primarily through U–Pb zircon geochronology of samples with clear relationships to known structural events. The age data are combined with information from extensive mapping (Ermanovics et al. 1989; Van Kranendonk 1990) and detailed structural and petrographic analysis (Van Kranendonk 1990, 1992*b*; Van Kranendonk and Ermanovics 1990; Ermanovics and Van Kranendonk 1990) to develop a model for the tectonic evolution of the Torngat Orogen.

Geology of the map area

The Torngat Orogen in the study area is broadly divided into three lithologic assemblages and four structural zones based on distinct rock associations and the orientation of structural fabric elements, respectively (Figs. 1, 2; references above).

Lithologic assemblages

(1) The Lac Lomier complex (LLC), located in the western part of the map area, is underlain by three lithologic units: (*i*) layered, tonalitic gneisses of probable Archean age (cf. Ryan 1990; Ryan et al. 1991) interpreted to be derived from protoliths of the southeastern Rae Province; (*ii*) quartzo-feldspathic paragneiss, quartzite, marble–calcsilicate and amphibolite gneiss interpreted to be derived from protoliths of the Early Proterozoic Lake Harbour Group (e.g., Jackson and Taylor 1972); and (*iii*) homogeneous charnockitic–enderbitic orthogneisses derived from calc-alkaline metaplutonic rocks (Iyer 1980; Schaumann 1987), interpreted as the remnants of an Early Proterozoic magmatic arc. All rocks of the complex are sheared under Early Proterozoic granulite- to amphibolite-facies metamorphic conditions. The complex is defined by a marked (up to +700 nT), north–south linear, total field aeromagnetic anomaly pattern, but its western limit is still unknown.

(2) The granulite-facies Tasiuyak gneiss complex (TGC), up to 40 km wide in the central part of the map area, is underlain by predominantly white, graphite-bearing, garnet–quartz–feldspar ± sillimanite gneiss (Fig. 2). This unit, known as the Tasiuyak gneiss (Wardle 1983), is interpreted to be derived from mainly graphitic, shaley sandstone protoliths deposited as a continental slope or accretionary prism on the thinned eastern margin of the southeastern Rae Province. The complex also includes isolated mafic to ultramafic bodies (≤100 m wide by 1–2 km long) and homogeneous charnockitic to enderbitic orthogneisses, identical to those extant in LLC. In the western part of the TGC, white garnetiferous, megacrystic perthite granite (S-type granite) and diatexitic migmatites occupy the cores of some folds (Fig. 2). The complex is marked by a low (as little as −700 nT), north–south linear, total field aeromagnetic pattern, which stands in marked contrast to the aeromagnetic high of the adjacent LLC.

(3) The eastern part of the map area is underlain by rocks that belong to the western margin of the Nain Province and were reworked within the Foreland zone of the Torngat Orogen (see below). In the eastern part of the zone, Archean gneisses intruded by Early Proterozoic tholeiitic Napaktok dykes are unconformably overlain by Early Proterozoic metasediments

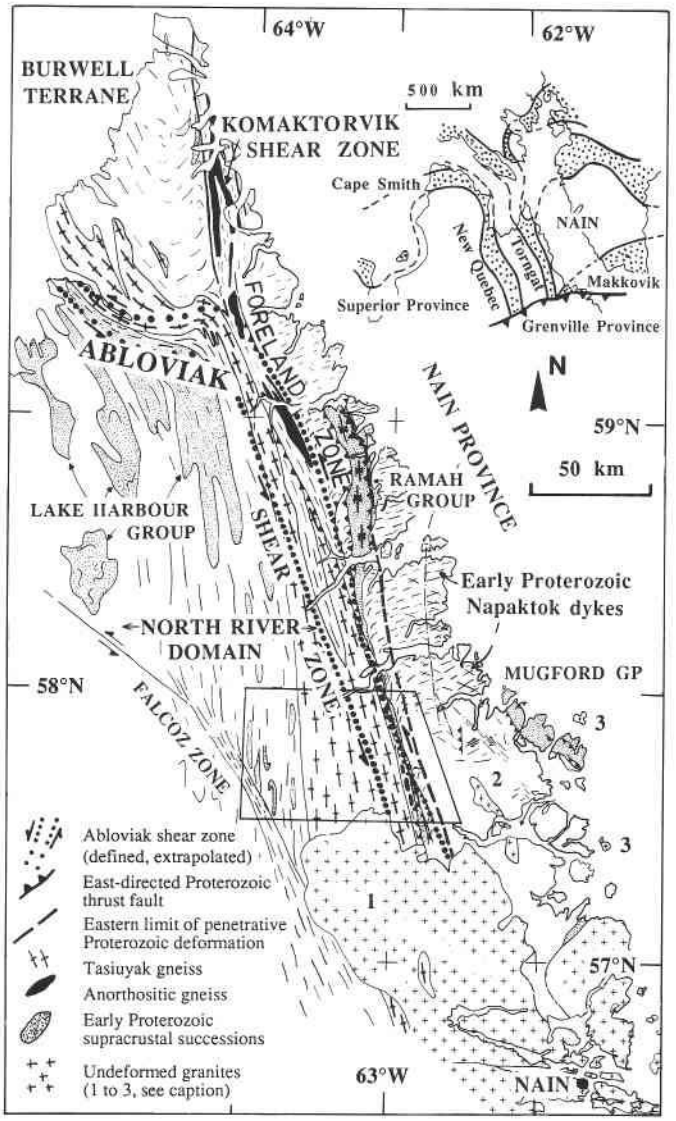

FIG. 1. Sketch map and location of the Torngat Orogen (from Van Kranendonk and Ermanovics 1990; insert from Hoffman 1990). Undeformed granites: 1, Elsonian intrusives; 2, Wheeler mountain; 3, Offshore Islands. Trapezoid outlines limits of Fig. 2.

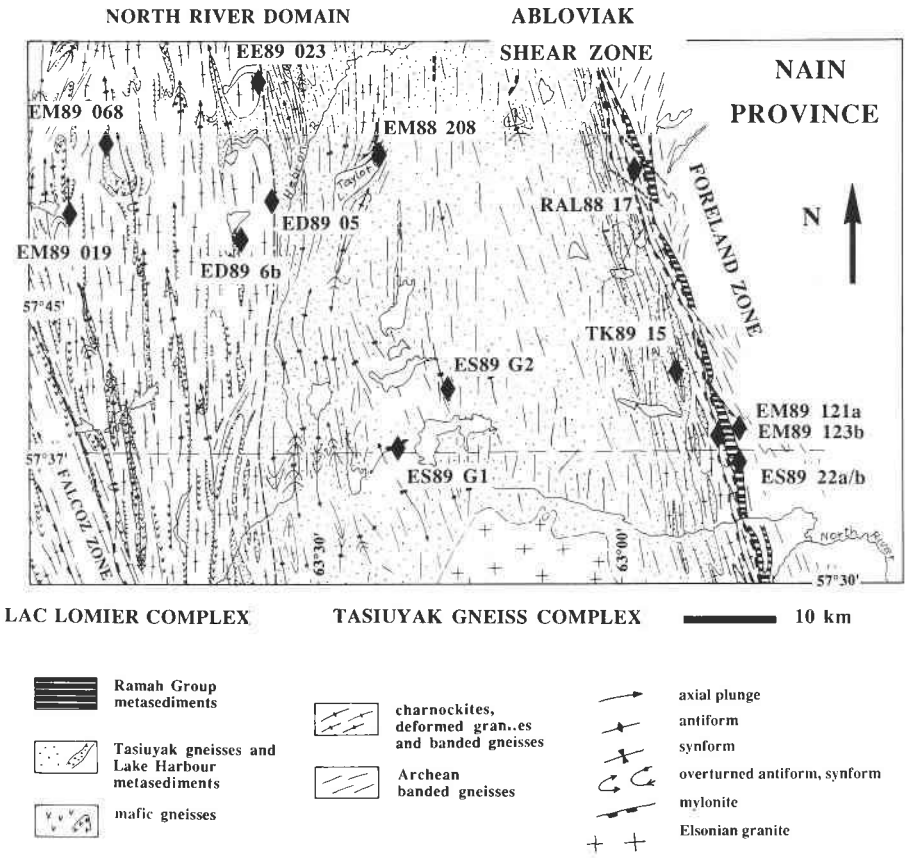

FIG. 2. Sketch map of North River – Nutak study area showing locations of samples (see Fig. 1 for map location).

of the Ramah Group and deformed at Early Proterozoic amphibolite facies (Fig. 2). Along the western margin of the Ramah Group, a set of steeply dipping, west-side-up mylonite to ultramylonite zones, 50–250 m wide, separate this area from a 0–4 km wide strip of Archean gneisses without dykes at Early Proterozoic granulite to amphibolite facies and rocks of the TGC.

Structural and metamorphic evolution

Extensive mapping and detailed structural studies (Van Kranendonk 1990, 1992*b*; Van Kranendonk and Ermanovics 1990) have led to the following model for the evolution of the orogen. *Stage 0*: Deposition of the protoliths of the shelf and slope deposits (Lake Harbour Group and Tasiuyak gneiss, respectively) on an east-facing flank of the southeastern Rae Province, and deposition of protoliths of Ramah Group on an opposing, west-facing flank of the Nain Province. This was followed by westward dipping subduction and the development of a magmatic arc in the southeastern Rae Province margin and in the protoliths of the Tasiuyak gneiss. *Stage I*: Initial continent–continent collision (D_1) leading to crustal thickening, nappe tectonics, and peak metamorphic conditions (P = 9–10 kbar (1 bar = 100 kPa), T = 950°C in the TGC). *Stage II*: Sinistral transpressive shearing (D_2) under continued high-grade metamorphic conditions, which is concentrated in the 10–12 km wide Abloviak shear zone (ASZ) (P = 7.3 kbar, T = 750–850°C in the ASZ). West of the ASZ, granulite-facies gneisses of the TGC and LLC are deformed into open, upright folds that trend north–south and have moderately north-plunging axes. In the reworked margin of the Nain Province to the east of the down-dip lineated mylonite zones, D_2 deformation occurred under amphibolite-facies conditions (Fig. 2). *Stage III*: Uplift of the orogen on subvertical, east-verging, low-grade mylonite faults (D_3) that are concentrated along the western margin of the Ramah Group at the transition from Early Proterozoic amphibolite- to granulite-facies metamorphic grade (Fig. 2). Pseudotachylite breccia veins are common within the mylonite zones, which become shallow west-dipping to the west within the TGC.

The three lithologic assemblages, defined above, are divided into four distinct structural zones, whose boundaries are based on the orientation of D_2 fabric elements, which all exhibit sinistral shear kinematics (Figs. 1, 2). From west to east these are (*i*) the 8–10 km wide, N160°-striking *Falcoz shear zone* at granulite- to amphibolite-facies metamorphic grade; (*ii*) the approximately 60 km wide *North River domain*, characterized by north–south striking, subvertical foliation planes and shallow to moderately north-plunging mineral lineations at granulite facies; (*iii*) the 10–12 km wide, N160° trending *Abloviak shear zone* (ASZ), developed within the eastern margin of the TGC and in the western margin of the Nain Province; and (*iv*) the 3–5 km wide *Foreland zone*, developed within the Nain Province, marking the eastern limit of penetrative Early Proterozoic deformation (Figs. 1, 2).

Previous geochronological data

The first indication that the Torngat Orogen might be Proterozoic in age was provided by a Rb–Sr whole-rock age of 1865 ± 40 Ma derived from granulites west of Hebron Fiord (F.C. Taylor in Wanless and Loveridge 1978). More recent studies from south of the present area confirm the existence of Proterozoic metamorphism and magmatic activity in the range 1860–1800 Ma and additionally demonstrate the presence of

reworked Archean rocks within the western part of the orogen (southeastern Rae Province, see Krogh 1990; Krogh and Heaman 1989; Ryan 1990; Ryan et al. 1991). $^{40}Ar/^{39}Ar$ hornblende ages from Saglek Fiord (Fig. 1) range between 1790–1750 Ma (Mengel et al. 1991), providing an age estimate for epeirogenesis.

Geochronological results from the Ungava and New Quebec orogens, west of the study area (Fig. 1), show that arc magmatism occurred from ca. 1898 to 1826 Ma, peak metamorphism from ca. 1845 to 1800 Ma, and final phases of deformation and epeirogenesis at ca. 1790–1750 Ma (Perreault and Hynes 1990; Machado et al. 1989; Parrish 1989; Lucas et al. 1992). Comparable geochronological data linking specific stages of orogeny were not available for the Torngat Orogen prior to this study (Bertrand et al. 1990).

Analytical methods

Sample preparation

U–Pb dating of zircon and monazite was carried out on 14 samples of pretectonic to syntectonic granitoid rocks from the main lithologic units and structural divisions of the Torngat Orogen in the North River map area (Fig. 2). After crushing, minerals were separated using heavy liquids, magnetic separation, and handpicking. Polished epoxy mounts of zircon were studied in detail, using both optical and scanning electron microscopy (SEM) in backscattered mode, before and after hydrofluoric acid etching of the surface. These studies enable the definition of individual zircon "populations" in different samples based on colour, morphology, and internal structure (Table 1). In some cases, half grains were removed from the mount and dated. A selection of SEM images of zircons and a monazite is presented in Fig. 3.

Nonmagnetic zircons of high quality were selected and all were abraded to minimize Pb loss (Krogh 1982). Single or several grain fractions were then selected from these abraded larger fractions to obtain the clearest grains with minimum fractures. In many samples, inheritance of core material in zircon is common. To date igneous events, attempts were made to physically separate cores from outer rims, although complete separation was not always possible and some grains probably retain more than one component. Three kinds of age figures are quoted in the text: $^{207}Pb/^{206}Pb$ ages of concordant to almost concordant fractions (<0.3% discordant); upper intercepts of discordia or reference lines determined from selected fractions; and $^{207}Pb/^{206}Pb$ model ages (>0.3% discordancy) given without error and interpreted as minimum ages.

Chemistry and mass spectrometry

Procedures for dissolution, separation, and purification of Pb and U using a $^{205}Pb-^{233-235}U$ mixed spike are given in Parrish et al. (1987). Total blanks for Pb during this study were between 5 and 22 pg for zircon and 17 and 58 pg for monazite. U blanks averaged 1 pg. Isotopic analyses were carried out on a Finnigan MAT 261 solid-source mass spectrometer equipped with multiple collectors and a secondary electron multiplier, and operating software designed for simultaneous static measurement of all five Pb isotopes (Roddick et al. 1987). Individual U–Pb analyses were corrected for common Pb using compositions derived from the Pb isotopic evolution curve of Stacey and Kramers (1975). Errors were propagated numerically (Roddick 1987) and are quoted in the text at the 2σ level. Discordia-line intercepts and associated errors were calculated using a modified York technique (York 1969) as described in Parrish et al. (1987). All ages were calculated using the decay constants of Steiger and Jäger (1977). Sample TK89 15 was analyzed at the Royal Ontario Museum.

$^{40}Ar/^{39}Ar$ analysis was carried out on hornblende of better than 99.5% purity after irradiation for 1.38 days in the fast neutron flux (2.3×10^{18} neutrons/cm^2) of the NRX reactor at Chalk River, Ontario, along with a laboratory hornblende monitor (PP-20). Complete procedures for $^{40}Ar/^{39}Ar$ analyses are detailed in Roddick (1990).

Sample descriptions and geochronological results

Four types of samples were collected for U–Pb dating: a sample of enderbitic gneiss to constrain the age of Early Proterozoic arc magmatism and subsequent deformation; samples of granitoid rocks interpreted to have been emplaced synkinematically with identified stages of deformation; samples of diatexite interpreted to have been derived through partial melting of country rocks during high-grade metamorphism accompanying deformation; and samples of weakly strained to undeformed granitoid rocks and pegmatites that crosscut high-grade deformation fabrics and thereby place minimum age constraints on identified stages of deformation. Hornblende was separated from the enderbite sample to estimate the time of cooling of the orogen. Together, this suite of samples should yield the full age range of Early Proterozoic magmatic and deformational events across the Torngat Orogen.

The results are presented as a description of the field setting of each sample, followed by descriptions of zircon populations according to shape, colour, and internal structure (Table 1) and the corresponding age data. Isotopic data are listed in Table 2 (a footnote explains the fraction labels).

Lac Lomier complex (LLC)

Enderbite (EE89 023)

This brown, homogeneous, enderbitic orthogneiss (hypersthene–hornblende–plagioclase–quartz) is in tectonic contact with Tasiuyak gneiss. It is representative of large, orthopyroxene-bearing metaplutonic bodies across the LLC and TGC, which are interpreted as the remnants of a preorogenic magmatic arc (Fig. 2). The sampled body contains strong, shallow north-plunging D_2 mineral lineations and a subvertical schistosity.

Nine different populations of zircon have been recognized in this sample (Table 1). Most of the needles (populations (pops.) 2, 4, 6) and flat zircons (pop. 7) contain no evidence of cores when viewed by SEM, but are characterized by an irregular, nebulitic, faint zoning (Fig. 3A). Some grains show a thin, probably low-U rim. In contrast, rounded and subhedral grains (pops. 8 and 9) show a bimodal structure of core and rim, only seen by SEM imagery, in which both components are transparent and devoid of zoning (Figs. 3B, 3C). Some of these cores (Fig. 3C) are reminiscent of partly resorbed flat zircon (pop. 7). This separation into two main zircon types is supported by their average uranium contents: 150–290 ppm for flat zircons and needles, and <50 ppm for rounded and subhedral grains.

Thirteen concordant or nearly concordant zircon fractions (Fig. 4A) are arrayed along concordia between 1876.9 ± 1.0 and 1822.5 ± 1.1 Ma. The oldest single zircon age ("flat" zircon fraction, pop. 7, A7-12, 0.31% discordant) is supported by the alignment of two other "flat" zircon fractions (pop. 7) and one needle (Amo4.1, pop. 4): regression of all four grains define a discordia with an upper intercept at 1883^{+66}_{-10} Ma (mean square weighted deviation (MSWD) = 6; Fig. 4A). Flat zir-

TABLE 1. Zircon populations

Sample	Pop.[a]	Shape	Colour[b]	Rims and cores	U (ppm)[c]	Analyses[d]	Fig. reference
Lac Lomier complex							
Enderbite	1	Long, rounded needles	Dark br	Late? outer shell, cores	Metamict	1	
(EE89 023)	2	Needles with rounded tips	Yel	Overg and cores	20	1	
	3	Rounded-shaped, multifacetted	Yel	Overg and cores	30–50	2	
	4	Long, striated needles, cracks	Yel, wh		290		
	5	Rounded, multifacetted balls	Yel, pk	Overg and cores			
	6	Subhedral needles, grading to 7	Pk, wh		150	1	
	7	Flat, disc-shaped grains	Col	Inclusions	170	3	3A
	8	Limpid round-shaped grains	Col	Overg and cores	20–50	3	3B, 3C
	9	Frag. of large subhedral grains	Col, pk	Overg and white cores	50	1	
Brown pegmatite	1	Large fragments	Pk, col	Overg from large grains	250	1	
(EM89 068)	2	Rounded to multifacetted		Overg and resorbed cores	300	1	
	3	Rounded subhedral needles			330	1	
Low-grade	1	Long, thin needles	Br				
Pegmatite	2	Slightly rounded prisms	Col, br		410	1	
(ED89 6b)	3	Flat grains	Col	No core grains	210	1	
Syntectonic	1	Needles with rounded angles	Br	Overg, fractured core	1230–2900	3	3D
Granite vein	2	Round-shaped grains	Pale br	Core and no core grains	200–2400	7	
(EM89 019)	3	Large frag. of euhedral grains	Col		340	1	
Red mylonite	1	Subhedral, rounded, short prisms	Col	Overg and resorbed cores	170–290	2	
(ED89 05)	2	Fractured needles, smooth angles	Pk		200	1	
	3	Shapeless rounded grains	Br	Overg, brown cores	550–1800	4	3F, 3G
Tasiuyak gneiss complex							
Anatectic	1	Long needles, smooth angles	Col, wh	Overg, resorbed cores	990–1700	7	3H
Tasiuyak granite	2	Rounded/multifacetted grains	Br	Overg, 5 to 60% core	1680–3220	4	3I
(ES89 G1)	3	Short, rounded bipyramids					
Hypersthene	1	Subhedral, rounded, short prism	Col		280	1	
Mobilizate	2	Round-shaped	Col	Zoned overg and cores	570–780	2	3J
(TK89 15)							
Tasiuyak	1	Multifacetted to rounded grains	Col, pk	Cores	180–615	8	3K
Leucogranite	2	Multifacetted to rounded (cracks)	Cloudy				
(Vein ES89 G2)	3	Short prisms, sharp pyramids	Cloudy				
	4	Thin, sharp euhedral needles	Col	Cores	560	1	
	5	Flat prisms with pyramids	Purple				
	6	Flat prismatic grains	Col				
Taylor lake	1	Round-shaped to "tailed"	Br	"Tail" overg, cores	220–580	2	3L, 3M
Granodiorite	2	Short to flat prisms	Pale yel	Overg and "ghost" cores	140	1	
(EM88 208)	3	Long euhedral needles	Col	No cores	60–115	2	
Pink deformed	1	Fragments	Col, br	Clear rims and br cores	50–220	4	
Granite	2	Euhedral needles	Br	Brown cores	160	1	
(RAL88 17)	3	Rounded grains	Br	Cores	820	1	
Western margin of Nain Province							
Down-dip deformed	1	Short bipyramids, rounded	Col	Cores	230	1	
Pegmatite	2	Multifacetted balls	Col	Cores	200	2	3N
(EM 89 121a)	3	Short prisms and bipyramids	Yel	Cores			
	4	Multifacetted balls	Cloudy	Some only core grains	140–220	2	
	5	Synneusis, outgrowths, etc.					
	6	Broken tips, fragments	Col	Only overg	100–230	2	
Ramah granite	1	Fragments	Col	Overg	130–270	2	
(ES89 22a)	2	Fragments	Col	Isolated cores	450	1	
	3	Short bipyramids	Col	Cores	400	1	
	4	Short bipyramids	Br, cloudy	Cores			
Ramah sillimanite	1	Short, euhedral prisms	Pale br	Pale brown, round cores			3O
Granite mylonite	2	Short, euhedral prisms	Pale br	No obvious cores			
(ES89 22b)	3	Fragments	Col	Overg and tips	410–1100	4	
	4	Rounded, multifacetted grains		Isolated cores?			
West Ramah	1	Transparent euhedral needles	Col				
Pegmatite	2	Needles full of microcracks	Cloudy				
(EM89 123b)	3	Large grains and fragments	Br	Outer shell, metamict cores	430–1150	4	3P

[a]Population numbers.
[b]col, colourless; pk, pink; br, brown; yel, yellow; wh, white; overg, overgrowth.
[c]Range or average from analyzed fractions.
[d]Number of analyzed fractions.

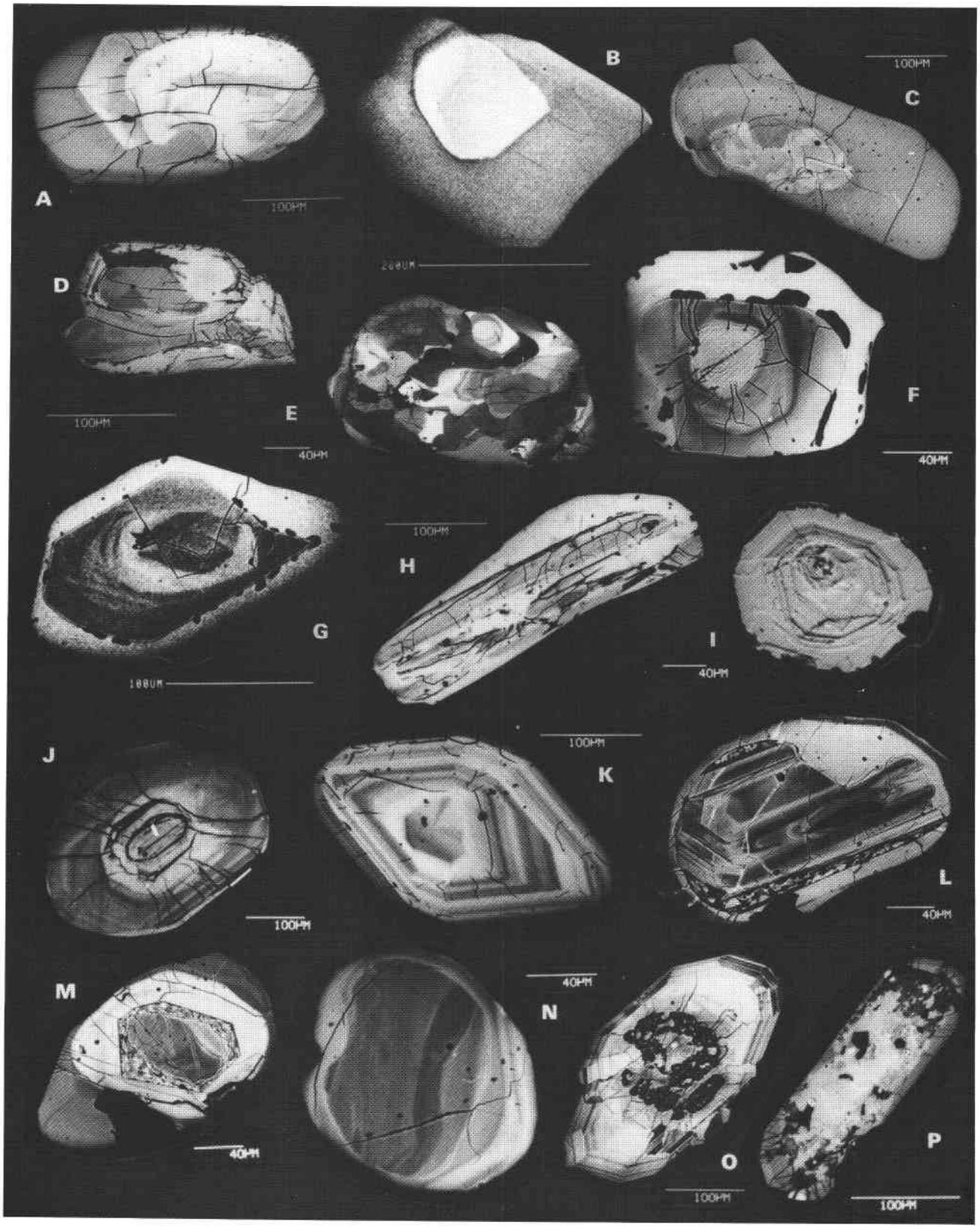

FIG. 3. Scanning electron microscope backscattered electron images of zircons (and one monazite, E) from the following locations: 1. Lac Lomier complex: (A–C) enderbite (EE89 023); (D, E) granite vein (EM89 019); (F, G) red mylonitic granite (ED89 05). 2. Tasiuyak Gneiss complex: (H, I) Tasiuyak anatectic granite (ES89 G1); (J) hypersthene mobilizate vein (TK89 15); (K) Tasiuyak leucogranite (ES89 G2); (L, M) Taylor Lake granodiorite (EM88 208). 3. Foreland zone: (N) down-dip deformed pegmatite (EM89 121a); (O) Ramah sillimanite granite mylonite (ES89 22b); (P) West Ramah pegmatite (EM89 123b). Grains D, F, G, H, I, K, L, M, N, O, and P are HF acid etched.

TABLE 2. U–Pb isotopic data

Fraction	Type	Wt. (μg)[a]	U (ppm)[a]	Pb (ppm)	U blank (pg)	Pb blank (pg)	*Pb analyzed (ng)[b]	(Th/U)[c]	$^{206}Pb/^{204}Pb$[d]	Pb_c (ppm)[e]	$^{206}Pb/^{238}U$ (%)	$^{207}Pb/^{235}U$ (%)	$^{207}Pb/^{206}Pb$ (%)	$^{207}Pb/^{206}Pb$ Age (Ma)	% Disc[f]
Z1731 EE89.023, enderbite, LLC, 57°50′N, 63°40′W															
Amo1.1	Fr Nd	32	162	54	0	8	1.7	0.239	10 692	0.1	0.3261±0.09	5.009±0.10	0.11141±0.03	1822.5±1.1	0.20
Amo2-31	Fr cores	364	20	7	0	9	2.4	0.179	6 694	0.0	0.3293±0.10	5.105±0.12	0.11244±0.03	1839.2±1.1	0.27
A3.1	no cores	59	30	10	1	11	0.6	0.140	2 022	0.1	0.3282±0.09	5.070±0.11	0.11205±0.05	1832.9±1.9	0.20
A3.2	Fr cores	21	49	16	1	13	0.4	0.207	656	0.9	0.3322±0.12	5.173±0.18	0.11294±0.13	1847.2±4.7	−0.11
Amo4.1	4 Nd	124	270	97	1	11	12.0	0.453	12 354	0.3	0.3344±0.08	5.266±0.10	0.11420±0.03	1867.3±1.1	0.47
Amo6.1	Fr Nd	110	140	48	1	5	5.3	0.323	34 095	0.0	0.3313±0.08	5.169±0.09	0.11316±0.03	1850.8±1.0	0.38
A7.1	flat	30	177	61	1	11	1.8	0.317	5 980	0.2	0.3322±0.08	5.210±0.10	0.11374±0.03	1860.1±1.2	0.69
Amo7.1	flat	151	162	57	1	10	8.7	0.361	16 465	0.1	0.3373±0.13	5.326±0.13	0.11453±0.03	1872.5±1.0	−0.07
A7-12	flat	70	181	64	1	10	4.5	0.348	19 989	0.0	0.3369±0.08	5.334±0.10	0.11481±0.03	1876.9±1.0	0.31
A8.1	cores	44	20	7	1	13	0.3	0.198	433	0.6	0.3318±0.12	5.143±0.25	0.11242±0.20	1838.8±7.1	−0.51
A8-12	cores	85	48	16	1	10	1.4	0.265	2 156	0.3	0.3279±0.09	5.063±0.11	0.11197±0.05	1831.7±1.8	0.21
Amo8-1	cores	277	20	7	0	6	1.8	0.170	15 165	0.0	0.3295±0.08	5.118±0.09	0.11263±0.03	1842.3±1.1	0.39
A9.1	Fr subh	48	56	18	0	9	0.9	0.236	2 884	0.2	0.3269±0.10	5.030±0.11	0.11160±0.04	1825.7±1.6	0.15
Z2197 EM89.068, brown pegmatite, LLC, 57°52′N, 63°52′W															
A1.2	Fr overg	121	252	97	0	10	11.8	0.823	38 887	0.0	0.3327±0.09	5.196±0.10	0.11328±0.03	1852.7±1.0	0.09
A2.1	3 cores	24	303	119	0	10	2.8	0.876	9 570	0.2	0.3320±0.09	5.190±0.10	0.11338±0.03	1854.2±1.2	0.37
A3.1	1 euh	23	335	131	0	10	3.0	0.850	2 016	2.8	0.3331±0.09	5.202±0.12	0.11327±0.05	1852.6±2.0	−0.04
MZA	5 Rd	85	347	6 370	0	58	541.5	216	4 756	0.8	0.3315±0.10	5.152±0.10	0.11272±0.04	1843.7±1.6	−0.11
Z2196 ED89.6b, low-grade pegmatite, LLC, 57°50′N, 63°40′W															
B2.1	1 euh	5	1104	412	0	10	2.1	0.688	9 844	0.3	0.3302±0.08	5.145±0.10	0.11302±0.03	1848.6±1.1	0.58
B3.1	2 flat	11	570	210	0	20	2.3	0.614	4 114	1.0	0.3314±0.09	5.184±0.10	0.11346±0.04	1855.5±1.3	0.66
Z1676 EM89.019, syntectonic granite vein, LLC, 57°50′N, 63°55′W															
B1.11	1 Nd	8	1638	493	2	14	3.8	0.199	2 268	11.0	0.2996±0.08	4.556±0.11	0.11028±0.05	1804.0±1.8	7.21
B1.12	1 Nd	10	2906	937	2	14	9.0	0.351	11 896	3.0	0.3090±0.08	4.735±0.10	0.11112±0.03	1817.9±1.0	5.14
C1.1	Nd	34	1340	427	2	14	14.3	0.293	4 858	4.6	0.3092±0.10	4.757±0.11	0.11158±0.04	1825.4±1.3	5.54
A2.1	1 Rd core	19	1964	565	1	13	11.0	0.256	1 921	16.0	0.2807±0.09	4.595±0.12	0.11873±0.06	1937.2±2.1	19.93
A2.3	1 Fr overg	2	1650	515	1	13	0.8	0.173	1 387	14.2	0.3128±0.09	4.789±0.12	0.11103±0.07	1816.4±2.4	3.89
B2.1	1 Rd, no core	10	2463	789	1	11	7.5	0.128	7 719	4.9	0.3243±0.09	4.992±0.10	0.11165±0.03	1826.4±1.1	0.99
B2.2	5 Rd	16	1242	418	1	11	6.6	0.289	20 253	0.5	0.3274±0.08	5.077±0.10	0.11249±0.03	1840.0±1.0	0.90
B2-a	1 Fr overg	4	618	200	0	7	0.8	0.230	4 993	0.6	0.3192±0.09	4.898±0.10	0.11127±0.04	1820.2±1.3	2.15
B2-b	1 core	4	222	84	0	9	0.3	0.846	783	3.1	0.3253±0.11	4.997±0.16	0.11142±0.11	1822.7±4.1	0.45
C2.1	9 Rd	20	1134	368	2	14	7.4	0.201	13 767	0.9	0.3221±0.08	4.958±0.10	0.11165±0.03	1826.4±1.0	1.67
A3.1	1 Fr overg	10	341	132	1	13	1.3	0.901	756	7.5	0.3274±0.09	5.038±0.17	0.11161±0.13	1825.7±4.6	−0.01
MZA	Rd	61	2093	8 579	0	18	521.6	44.80	34 201	0.9	0.3346±0.22	5.217±0.23	0.11310±0.03	1849.8±1.0	−0.66
MZ2	2 Rd	7	2465	12 922	0	37	87.9	58.80	6 717	2.0	0.3320±0.09	5.152±0.10	0.11255±0.03	1841.1±1.2	−0.43
Z1744 ED89.05, red mylonite, LLC, 57°50′N, 63°36′W															
A1.2	1 subh	11	271	101	1	10	1.1	0.753	5 217	0.1	0.3270±0.12	5.034±0.13	0.11164±0.04	1826.3±1.5	0.15
A1.3	subh	39	170	60	0	7	2.3	0.531	15 064	0.0	0.3263±0.08	5.025±0.10	0.11168±0.03	1827.0±1.0	0.40
A2.1	Fr overg?	4	202	70	0	6	0.3	0.470	2 061	0.3	0.3254±0.12	5.003±0.13	0.11150±0.07	1823.9±2.5	0.49
A3-12	1 core	8	655	165	1	140	1.3	0.346	497	2.6	0.2413±0.17	3.729±0.26	0.11208±0.21	1833.4±7.5	26.66
A3.21	1 core?	10	547	178	0	9	1.9	0.209	7 869	0.5	0.3232±0.08	4.959±0.10	0.11128±0.03	1820.5±1.2	0.96
A3.31	1 core	5	1810	614	1	10	3.2	0.291	9 537	1.8	0.3295±0.09	5.104±0.11	0.11233±0.03	1837.5±1.1	0.08
A3.43	1 core	6	1205	417	0	20	2.5	0.401	5 069	1.4	0.3273±0.08	5.058±0.10	0.11208±0.03	1833.5±1.2	0.52
MZA	Rd	43	1030	6 027	0	35	257.9	67.90	23 193	0.1	0.3233±0.09	4.935±0.10	0.11073±0.03	1811.4±1.1	0.36

TABLE 2 (*continued*)

Fraction	Type	Wt. (μg)[a]	U (ppm)[a]	Pb (ppm)	U blank (pg)	Pb blank (pg)	*Pb analyzed (ng)[b]	(Th/U)[c]	$^{206}Pb/^{204}Pb$[d]	Pb_c (ppm)[e]	$^{206}Pb/^{238}U$ (%)	$^{207}Pb/^{235}U$ (%)	$^{207}Pb/^{206}Pb$ (%)	$^{207}Pb/^{206}Pb$ Age (Ma)	% Disc[f]
Z1719 ES89 G1, Tasiuyak anatectic granite, TGC, 57°37′N, 63°23′W															
B1.1	Nd	50	1 273	413	0	8	20.4	0.226	15 589	1.4	0.3197±0.09	5.014±0.10	0.11373±0.03	1859.9±1.0	4.40
B1.21	1 Nd	9	1 070	354	1	13	3.0	0.199	8 735	0.9	0.3288±0.08	5.155±0.10	0.11370±0.03	1859.4±1.1	1.65
B1.22	1 Nd	9	1 704	523	0	6	4.7	0.111	13 865	1.6	0.3115±0.09	4.893±0.10	0.11389±0.03	1862.5±1.0	6.99
B1.23	1 Nd	14	1 161	370	0	6	5.1	0.164	11 068	1.5	0.3189±0.08	4.997±0.10	0.11365±0.03	1858.6±1.1	4.57
B1.31	1 Nd	12	1 287	432	1	13	5.0	0.357	9 251	1.5	0.3205±0.08	4.965±0.10	0.11235±0.03	1837.7±1.1	2.83
D1.11	5 Nd	11	1 364	427	0	11	4.5	0.138	7 429	2.4	0.3155±0.08	4.938±0.10	0.11351±0.03	1856.3±1.1	5.46
D1.12	5 Nd	10	1 452	452	0	11	4.7	0.0983	15 639	0.7	0.3174±0.09	4.932±0.10	0.11270±0.03	1843.4±1.0	4.12
A2.1	Rd	41	2 248	727	0	8	29.8	0.127	92 074	0.3	0.3270±0.10	5.089±0.11	0.11288±0.03	1846.3±1.0	1.40
A2.11	Rd	15	3 486	1 123	1	13	16.6	0.0738	39 088	0.9	0.3303±0.09	5.134±0.10	0.11273±0.03	1843.9±1.0	0.26
B2.21	Rd	19	2 054	652	1	13	12.1	0.177	10 770	2.9	0.3169±0.08	4.915±0.10	0.11248±0.03	1839.9±1.1	4.04
D2.1	Rd	27	1 819	555	0	8	14.7	0.102	17 566	1.6	0.3110±0.09	4.798±0.10	0.11190±0.03	1830.5±1.0	5.29
MZA	Rd	46	8 885	17 777	0	18	824.9	20.50	85 512	1.6	0.3270±0.29	5.099±0.29	0.11307±0.03	1849.4±1.0	1.57
MZ2	1 Rd	2	13 088	23 007	0	37	43.7	17.20	10 112	6.8	0.3328±0.09	5.211±0.10	0.11356±0.03	1857.1±1.1	0.30
TK89 15, hypersthene mobilizate vein, TGC, 57°42′N, 62°58′W															
RP1	1 Rd	est. 7	780	298			2.1	0.745	8 980	1.9	0.3331±0.5	5.214±0.5	0.11352±0.1	1856±3.6	0.19
RP2	1 Rd	est. 11	573	197			2.2	0.294	9 549	1.3	0.3330±0.5	5.221±0.5	0.11371±0.1	1859±3.6	0.39
IC1	1 Nd	est. 5	281	97			0.5	0.299	1 810	3.3	0.3308±0.5	5.143±0.5	0.11275±0.1	1844±3.6	0.09
Z1763 ES89 G2, Tasiuyak leucogranite vein, TGC, 57°40′N, 63°15′W															
A1.1	2 no cores	17	276	89	1	10	1.5	0.221	8 483	0.0	0.3190±0.09	4.809±0.10	0.10932±0.03	1788.2±1.2	0.21
(-)1A1.2	2 cores	79	615	205	0	20	16.2	0.375	8 494	1.1	0.3175±0.08	4.796±0.10	0.10954±0.03	1791.8±1.1	0.90
A1.3	6 no cores	56	203	66	0	7	3.7	0.277	24 418	0.0	0.3182±0.08	4.802±0.10	0.10943±0.03	1789.9±1.0	0.56
Am1-11	1 no cores	23	197	65	0	9	1.5	0.339	8 991	0.0	0.3186±0.10	4.802±0.11	0.10933±0.03	1788.3±1.1	0.36
Am1.12	2 no cores	19	430	136	1	10	2.5	0.157	9 968	0.3	0.3191±0.08	4.809±0.10	0.10931±0.03	1787.9±1.1	0.16
Am1.141	1 core	14	265	87	0	9	1.2	0.3	5 190	0.3	0.3195±0.09	4.822±0.10	0.10948±0.04	1790.7±1.3	0.23
Am1.142	1 core	13	375	120	1	10	1.5	0.204	3 315	1.4	0.3194±0.10	4.815±0.11	0.10932±0.04	1788.0±1.5	0.07
Am1.41	3 Nd	28	605	205	0	9	5.7	0.448	11 089	0.7	0.3174±0.11	4.795±0.12	0.10958±0.03	1792.4±1.1	0.99
MZA		58	405	5 342	0	35	308.2	162	6 308	0.6	0.3155±0.10	4.736±0.11	0.10887±0.03	1780.5±1.3	0.82
Z1928 EM88 208, Taylor Lake granodiorite, TGC, 57°52′N, 63°22′W															
B1.1	1 Rd core	12	223	76	0	7	0.9	0.238	6 430	0.1	0.3361±0.09	5.334±0.10	0.11509±0.03	1881.3±1.2	0.81
C1.1	cores	5	581	185	0	22	0.9	0.266	1 864	1.6	0.3114±0.09	4.716±0.11	0.10983±0.06	1796.7±2.1	3.11
B2.1	tips + Fr	23	137	63	0	22	1.4	0.452	1 635	1.1	0.4138±0.10	8.917±0.11	0.15629±0.05	2415.9±1.7	8.98
C3-0	3 Nd	8	59	20	0	12	0.2	0.486	742	0.1	0.3174±0.14	4.807±0.20	0.10983±0.15	1796.6±5.6	1.24
C3.1	Nd + tips	8	114	39	0	14	0.3	0.444	1 083	0.4	0.3194±0.11	4.829±0.15	0.10965±0.10	1793.7±3.6	0.44
MZ		9	173	1 371	0	40	11.9	97.60	505	2.1	0.3086±0.14	4.536±0.23	0.10659±0.18	1742.0±6.7	0.52
Z1559 RAL88 17, pink deformed granite, Foreland, 57°52′N, 63°00′W															
A1-1	1 euh, core?	12	132	82	5	14	1.0	1.390	2 658	0.3	0.4607±0.13	10.836±0.14	0.17059±0.04	2563.5±1.2	5.66
B1-1	1 euh	4	46	27	5	14	0.1	3.260	198	1.5	0.3273±0.94	5.006±1.0	0.11095±0.47	1815.0±17.2	−0.64
B1-2	13 euh tips	24	71	29	0	8	0.7	1.1	1 891	0.4	0.3286±0.09	5.169±0.11	0.11406±0.05	1865.2±1.9	2.05
C1-1	7 fr euh	5	221	83	5	14	0.4	0.8	550	5.1	0.3224±0.18	4.907±0.25	0.11039±0.15	1805.8±5.5	0.27
B2-1	7 euh + overg	14	162	65	0	8	0.9	1.220	4 319	0.2	0.3183±0.09	4.843±0.10	0.11033±0.04	1804.8±1.4	1.47
B3-1	1 Rd	5	823	433	0	8	2.2	0.298	2 841	6.3	0.4846±0.11	11.889±0.12	0.17792±0.04	2633.6±1.4	3.96

TABLE 2 (*concluded*)

Fraction	Type	Wt. (μg)[a]	U (ppm)[a]	Pb (ppm)	U blank (pg)	Pb blank (pg)	*Pb analyzed (ng)[b]	(Th/U)[c]	$^{206}Pb/^{204}Pb$[d]	Pb_c (ppm)[e]	$^{206}Pb/^{238}U$ (%)	$^{207}Pb/^{235}U$ (%)	$^{207}Pb/^{206}Pb$ (%)	$^{207}Pb/^{206}Pb$ Age (Ma)	% Disc[f]
Z1843 EM89 121a, down-dip deformed pegmatite, Foreland, 57°39′N, 62°50′W															
B1.1	core	24	228	89	1	10	2.1	0.311	1 332	3.2	0.3699±0.15	7.275±0.17	0.14265±0.07	2259.6±2.3	11.89
B2.1	core	21	186	71	1	10	1.5	0.249	3 268	0.7	0.3674±0.08	7.392±0.10	0.14590±0.04	2298.4±1.2	14.23
Am1.21	core	22	203	111	1	7	2.4	0.444	14 482	0.1	0.4787±0.08	13.710±0.10	0.20772±0.03	2887.9±0.9	15.30
B4.1	core	13	218	100	1	10	1.3	0.597	1 211	3.4	0.4049±0.11	8.446±0.14	0.15129±0.07	2360.6±2.3	8.44
Am1.41	3 cores	17	138	56	0	20	0.9	0.271	1 669	0.7	0.3820±0.09	8.128±0.11	0.15434±0.05	2394.6±1.6	15.09
B6t.1	tips	7	257	97	0	10	0.7	0.143	3 851	0.1	0.3701±0.09	7.417±0.10	0.14535±0.04	2291.9±1.2	13.31
B6t.2	3 tips	5	617	211	0	20	1.1	0.114	2 150	2.0	0.3423±0.09	5.991±0.11	0.12691±0.05	2055.6±1.6	8.85
MZA	flat ± Rd	57	1160	5140	0	17	292.5	51.60	14 250	1.2	0.3162±0.11	4.726±0.12	0.10842±0.03	1773.1±1.1	0.14
Z2198 ES89 22a, Ramah granite, Foreland, 57°37′N, 62°50′W															
(-)1B1-1	Fr overg?	28	131	59	0	10	1.6	0.197	5 535	0.2	0.4241±0.09	9.914±0.10	0.16955±0.03	2553.2±1.2	12.73
(-)1B1.2	Fr overg?	8	273	111	0	20	0.9	0.308	1 040	3.5	0.3832±0.09	7.882±0.12	0.14919±0.07	2336.7±2.3	12.29
(-)1B2.2	1 core	8	449	154	0	10	1.2	0.130	5 165	0.6	0.3424±0.09	5.916±0.10	0.12530±0.03	2033.0±1.0	7.64
(-)1B3.1	2 cores	7	404	173	0	10	1.2	0.234	5 640	0.3	0.4033±0.09	9.268±0.10	0.16666±0.03	2524.4±1.0	15.86
MZB	5 euh	15	2476	3438	0	58	51.6	14.10	5 866	3.9	0.3075±0.08	4.513±0.10	0.10643±0.03	1739.1±1.2	0.69
Z1759 ES89 22b, Ramah sillimanite-granite mylonite, Foreland, 57°37′N, 62°50′W															
A3.1	2 overg	14	632	193	0	9	2.7	0.0396	9 899	0.6	0.3177±0.08	4.781±0.10	0.10916±0.03	1785.4±1.1	0.46
A3.2	overg	10	1010	307	0	9	3.0	0.0326	7 906	1.5	0.3167±0.09	4.771±0.10	0.10926±0.03	1787.2±1.2	0.88
B3.1	tip	7	409	139	1	10	1.0	0.150	2 629	1.7	0.3389±0.10	5.740±0.11	0.12282±0.04	1997.6±1.6	6.70
B3.2	tip	7	1106	335	1	10	2.3	0.0445	7 832	1.2	0.3134±0.09	4.759±0.10	0.11016±0.03	1802.0±1.1	2.84
MZA	euh	56	3346	7181	0	18	403.5	22.80	35 112	1.5	0.3196±0.23	4.800±0.24	0.10893±0.03	1781.6±1.0	−0.39
Z1927 EM89 123b, west Ramah deformed pegmatite, Foreland, 57°39′N, 62°50′W															
A3-1	1 subh	11	1142	340	0	18	3.7	0.0301	11 519	0.3	0.3101±0.09	4.676±0.10	0.10935±0.03	1788.6±1.2	3.02
A3-2	Fr	6	1076	329	0	8	2.0	0.045	12 238	0.3	0.3170±0.08	4.775±0.10	0.10926±0.03	1787.1±1.1	0.78
B3-1	tips	10	431	124	0	8	1.2	0.0335	8 263	0.2	0.3002±0.08	4.485±0.10	0.10835±0.03	1771.8±1.1	5.09
B3-21	1 tip	9	889	282	0	12	2.5	0.0278	11 126	0.3	0.3306±0.09	5.007±0.10	0.10986±0.03	1797.1±1.1	−2.82

NOTES: Zircon fractions are labelled according to their size and magnetic properties (except for sample TK89 15): A > 150 μm; B = 150−100 μm; C = 100−75 μm; D < 75 μm. A simple letter means a nonmagnetic fraction at 0°, 1.7 A (except for Z2196, Z2197, Z2198 = 0°, 3.5 A). Fractions with (-) are diamagnetic. Magnetic fractions are quoted mo and m1 (0° and 1°, respectively). a and b in fraction number correspond to grains removed from epoxy mounts after SEM imaging. Rd, round shaped; Nd, needle; overg, overgrowth; Fr, fragment; euh, euhedral; subh, subhedral; MZ, monazite. Errors are 1 SE of mean in % except $^{207}Pb/^{206}Pb$ age errors which are 2 SE in Ma.

[a]Include sample weight error of ±0.001 mg in concentration uncertainty.

[b]Analyzed radiogenic Pb.

[c]Th/U from 208*/206* and 207*/206* age.

[d]Measured $^{206}Pb/^{204}Pb$ in an analysis, including Pb blank.

[e]Common Pb concentration in sample.

[f]Discordance on cord to origin.

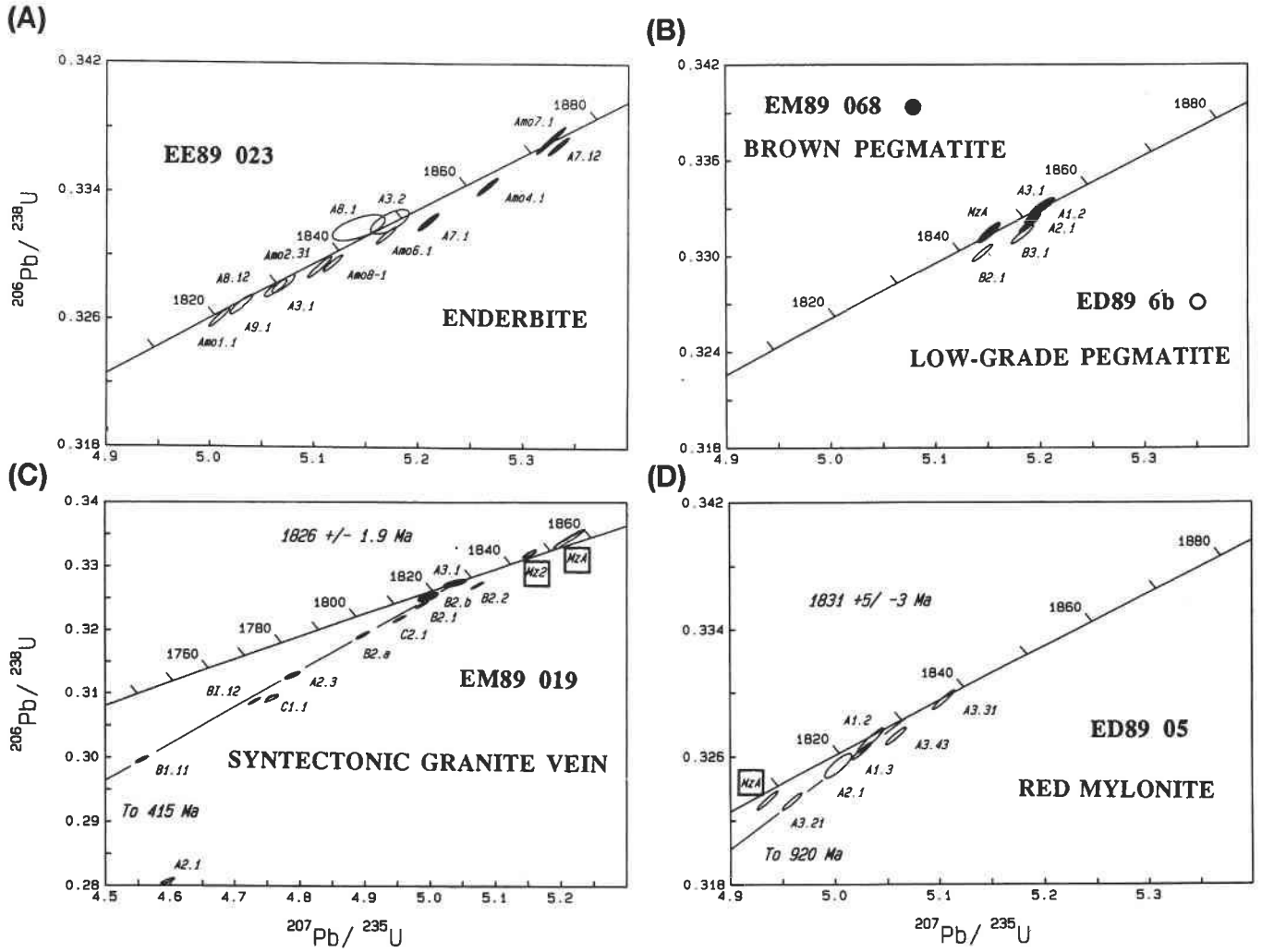

FIG. 4. Lac Lomier complex $^{206}Pb/^{238}U$ vs. $^{207}Pb/^{235}U$ diagrams. (A) Enderbite (EE89 023); "flat" zircons of population 7 and an intermediate needle are in black. (B) Brown pegmatite (EM89 068), filled ellipses; low-grade pegmatite (ED89 6b), two open ellipses. (C) Syntectonic granite vein (EM89 019); filled ellipses correspond to the calculated discordia. (D) Red mylonitic granite (ED89 05). All error ellipses are 2σ.

cons form the largest population in the rock (about 60%). Their unusual flat and rounded disc shape is interpreted to result from rounding of Pupin's type S25 (Pupin 1980), initially crystallized at magmatic temperatures. Rounded angles and lack of overgrowths reflect their early crystallization during emplacement of the enderbite (ca. 1877 Ma).

A fraction of large subhedral zircons from pop. 9 (A9-1, 0.15% discordant) yields an age of 1825.7 ± 1.6 Ma. Despite their subhedral morphology, and because no evidence exists for melting during high-grade deformation of the orthogneiss (little or no leucosome material), this type of unzoned, low-U zircon probably dates the time of metamorphic crystallization.

The youngest concordant age of 1822.5 ± 1.1 Ma is from the outer rim of probably older, metamict zircon grains (clear fragments, pop. 1, Amo1-1, 0.2% discordant). It is slightly younger (3 Ma) than the inferred metamorphic age and may represent the last stages of zircon growth.

The other slightly discordant fractions from pops. 3, 8, and 9, which lie along and just below concordia, are interpreted as reflecting variable effects of lead loss or partial recrystallization of cores during metamorphism. Such an interpretation is supported by the similarity between nebulitic zoning in the flat zircons (pop. 7, Fig. 3A) and irregular patches observed in large subhedral grains (pops. 8 and 9, Fig. 3C).

A $^{40}Ar/^{39}Ar$ analysis on hornblende from this sample yields an apparent plateau age of 1734 ± 11 Ma (Fig. 5) which represents the time of cooling below amphibolite facies temperatures in the central part of the orogen.

Brown pegmatite (EM89 068)

This 5 m wide, east–west striking granite pegmatite dyke is located in a low-strain lozenge (5 × 3 km) about 15 km west of the TGC boundary (Fig. 2). The dyke cuts across north-south striking, D_1 gneissosity in Early Proterozoic metasediments and is undeformed except for a weak, subvertical north–south fracture cleavage, interpreted as a D_2 structure. It contains mesoperthite and retrogressed orthopyroxene, suggesting metamorphism at granulite facies and subsequent retrogression to amphibolite facies. The pegmatite is interpreted as having been emplaced during late stages of stage I (granulite facies) then retrogressed and mildly deformed during stage II.

Three fractions from three different zircon populations (Table 1) were analyzed and yield similar, concordant to almost concordant ages (Table 2, Fig. 4B): (*i*) a subhedral needle

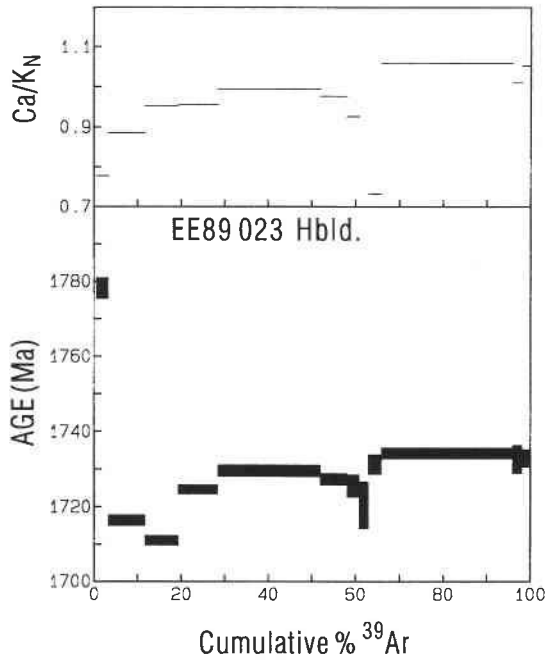

FIG. 5. $^{40}Ar/^{39}Ar$ spectrum on hornblende from enderbite EE89 023. Errors on individual steps are shown at 2σ.

with smooth angles (A3-1, single grain pop. 3) yields a concordant age of 1852.6 ± 2.0 Ma; (*ii*) a large, homogeneous fragment (pop. 1) at 1852.7 ± 1.0 Ma (A1-2, 0.1% discordant) is identical, within error, to A3-1 above; and (*iii*) colourless core fragments from multifaceted grains (pop. 2) yield a similar age of 1854 Ma (A2-1, 0.4% discordant). Concordant, rounded, anhedral monazite is significantly younger at 1843.7 ± 1.6 Ma.

The zircon and monazite data from this sample may be interpreted in two ways. In the first interpretation, the zircon age (ca. 1853 Ma) represents the time of pegmatite intrusion (a minimum age of stage I deformation), and the younger monazite age represents closure of the monazite system at about 725°C (Parrish 1990) during protracted cooling following stage I. A second, but less preferred interpretation is that the monazite dates the actual emplacement age of the pegmatite, and that the zircons are xenocrysts inherited from the metamorphosed country rocks. In either case, because the zircon ages are younger than the age of intrusion of the pretectonic enderbite (EE89 023), the zircon data is interpreted to reflect the age of the metamorphic peak associated with stage I crustal thickening. The monazite date suggests that granulite facies metamorphic temperatures did not affect this sample after 1844 Ma.

Low-grade pegmatite (ED89 6B)

This amphibolite-facies pegmatite from the eastern margin of the LLC is 2 m wide by >30 m long and crosscuts the main D_2 fabric elements in gneisses of the North River domain. The pegmatite contains a low-grade, north–south striking schistosity (D_2) and is interpreted as postdating stage I.

Two zircon fractions from three defined populations have been analyzed (Table 1 and 2, Fig. 4B) and both are discordant: "flat", disc-shaped zircons with no cores (B3-1, pop. 3) yield a $^{207}Pb/^{206}Pb$ age of 1855 Ma (0.66% discordant); and a short subhedral colourless prism (B2-1, pop. 2) yields a $^{207}Pb/^{206}Pb$ age of 1849 Ma (0.58% discordant).

The fact that this sample postdates D_1 deformation (dated as ca. 1854 Ma in the above samples) suggests that the zircon fractions probably represent xenocrysts inherited from country rocks metamorphosed during stage I and that the age of emplacement of this pegmatite is unknown.

Syntectonic granite vein (EM89 019)

This 50 cm wide by >10 m long, pink, microcline-bearing granitic vein is located south–southwest of the brown pegmatite (EM89 068) in the LLC (Fig. 2). It cuts the regional metamorphic layering at a low angle but has a subvertical foliation and an intermediate north-plunging lineation (025°/36°), both of which are subparallel to regional D_2 fabric elements. This granite vein, emplaced under amphibolite facies conditions, is interpreted to be synkinematic to late kinematic with respect to stage II.

Three populations of zircon were analyzed in this sample (Table 1): (*i*) Three fractions of brown needles containing thin, bone-shaped, fractured cores sometimes associated in synneusis (pop. 1, Fig. 3D) are scattered along a poorly defined discordia line (B1-11, B1-12, and C1-1, the latter multigrained; Fig. 4C). (*ii*) Seven fractions of pale brown rounded grains (pop. 2); SEM images confirm that many grains are completely devoid of cores and represent only a finely-zoned magmatic growth. Two fractions are fragments of outer, finely zoned overgrowths: A2-3, a fragment broken during abrasion from a >150 μm grain, and B3-a, a fragment removed from an epoxy mount after SEM analysis. Fractions B2-1, B2-2, and C2-1 represent mixed grains with dominant overgrowths. Fractions A2-1 and B2-b are clearly cores: A2-1 is a 20% discordant fraction (not shown on Fig. 4*c*) and B2-b is from an epoxy mount. This population, except for A2-1, is scattered along the array together with pop. 1. (*iii*) One large limpid fragment of an euhedral grain (pop. 3, A3-1) is concordant at 1825.7 ± 4.6 Ma and at the upper end of the array of pops. 1 and 2 (Fig. 4C).

A discordia calculated using 5 single grain analyses (B1-11, A2-3, B2-a, B2-b, and A3-1) has an upper intercept age of 1826 ± 2 Ma and a lower intercept at ca. 415 Ma (MSWD = 0.7). The coincidence of fragments and cores along the same discordia suggests that some cores are either very close in age to the magmatic overgrowths or that they have been reset. The upper intercept of the discordia is well constrained by the concordant fraction A3-1 at 1825.7 ± 4.6 Ma and this age is interpreted as the time of granite vein emplacement. Fraction A2-1, with a $^{207}Pb/^{206}Pb$ age of 1937 Ma (Table 2), indicates that some cores are inherited.

Two monazite fractions overlap concordia at 1849.8 ± 1.0 Ma (−0.66% discordant) and 1841.1 ± 1.2 Ma (−0.43% discordant). They are older than the $^{207}Pb/^{206}Pb$ ages of all zircon fractions, except core A2-1. In SEM backscattered electron images, anhedral monazite shows a complex, patchy structure suggestive of postcrystallization element mobility (Fig. 3E). This morphology has also been observed by Parrish (1990) in inherited monazite. The monazites in the present sample are thus interpreted to be partially reset monazite, inherited from the surrounding gneisses.

Red mylonitic granite (ED89 05)

This strongly deformed red granite is only known from the transition zone between LLC and TGC, where stage II deformation is locally concentrated. The sample is a mesoperthite- and hornblende-bearing granitoid rock, which outcrops intermittently as dykes or small stocks throughout an area 1 km wide and ≥ 10 km long. The granitoid intrusions were probably emplaced under granulite-facies conditions and subsequently

deformed and retrogressed to amphibolite facies during stage II.

Seven zircon fractions were analyzed from the three populations defined in this sample (Table 1, Fig. 4D): (*i*) Two fractions of subhedral, rounded grains, which contain small, resorbed cores; one of these, A1-2 is nearly concordant (0.15% discordant) at an age of 1826.3 ± 1.5 Ma. (*ii*) One fraction (A2-1) of fragments of highly cracked, short needles with rounded angles (pop. 2), believed to represent outer zones (overgrowth?) rather than cores, yields a $^{207}Pb/^{206}Pb$ age of 1824 Ma (0.49% discordant). (*iii*) Four fractions of cores from rounded grains (pop. 3) have metamorphic rims (e.g., Figs. 3F, 3G) that were removed through abrasion prior to analysis; one brown core yields the oldest age of 1837.5 ± 1.1 Ma (A3-31, 0.08% discordant); another, more discordant core (A3-43, 0.52% discordant) has a similar U content and a slightly younger $^{207}Pb/^{206}Pb$ age of ca. 1833 Ma. Two other fractions are more discordant (0.96%, 27%: Fig. 4D). These cores are interpreted to date the igneous age of the granite.

The needle fragments and cores appear to be similar in age and a four-point discordia defined by two subhedral grains, needle fragments, and one core yields an age of 1830^{+5}_{-3}. The almost concordant age of 1826.3 ± 1.5 Ma (A1-2) is a more precise estimate of the main recrystallization–deformation event that affected the sample (stage II). As field and microscopic evidence preclude a syntectonic emplacement for this rock, the similarity in age of the recrystallization event in this sample and the last event recognized in the enderbite suggests that metamorphic zircon growth was superimposed upon magmatic cores at ca. 1826 Ma. Rounded monazite yields an almost concordant age of 1811.4 ± 1.1 Ma (0.36% discordant), interpreted as the age of cooling below the monazite blocking temperature of approximately 725°C (Parrish 1990).

Tasiuyak gneiss complex (TGC)

Anatectic Tasiuyak granite (ES89 G1)

This white, heterogeneous garnet–perthite–biotite granite was sampled from the weakly foliated and lineated migmatitic apron of a more homogeneous perthite-megacrystic granite. Such granites range from 0.1 to 2 km in diameter and occupy structural domes in areas of openly folded and shallowly-dipping Tasiuyak gneiss west of the ASZ (Fig. 2). The granites are interpreted as S-type, synkinematic to late-kinematic intrusions related to the crustal thickening (stage I), which were deformed and partly recrystallized (remelted?) during stage II deformation.

Two of the three zircon populations identified in this sample were analyzed (Table 1, Fig. 6A). Most grains examined by SEM are rimmed by a dark, corrugated, finely-banded alteration zone rich in Fe and Ca (Fig. 3I), which also fills cracks. This alteration enhances the brown colour of the grains but was easily removed from the analyzed fractions during abrasion.

Pop. 1 consists of needles showing a clear discontinuity between a finely zoned envelope and a highly fractured core (Fig. 3H). The younger envelope material also infiltrates the cores leaving long septae resembling "bones" within the grains (Fig. 3H; cf. Black et al. 1986). Abrasion did not remove all of this rim and infiltrated material prior to complete disaggregation of the grains. Abraded needle fractions therefore represent a concentration of core material (~90%). Seven fractions of these needles have been analyzed; all are highly discordant. Five of the fractions define a discordia yielding an age of 1858 Ma (MSWD = 21), identical within error to an almost concordant (0.30% discordant), anhedral monazite grain at 1857.1 ± 1.1 Ma (Fig. 6A). Assuming a closure temperature of monazite of 725°C (Parrish 1990), this age may correspond either to the crystallization age of an "old" Tasiuyak anatectic granite or to its metamorphic protolith. The age is in good agreement with that of sample EM89 068, and together these data are used to infer the time of stage I deformation and granulite-facies metamorphism across the orogen. Two remaining needle fractions (B1-31, D1-12) are also discordant but have younger $^{207}Pb/^{206}Pb$ ages, similar to that of rounded zircons (see below); they probably correspond to grains dominated by infiltrated rim material.

Pop. 2 corresponds to brown, rounded zircon grains. SEM images of HF-etched grains show that most contain only a tiny remnant core or no core (Fig. 3I), and irregular, fine zoning similar to magmatic zoning. Four core-free fractions are all U-rich (1800–3500 ppm). One almost concordant fraction (A2-11, 0.26% discordant) is the youngest at 1843.9 ± 1.0 Ma and dates the last crystallization event (Fig. 6A). This age is supported by a poorly defined five-point discordia (D2-1, B2-21, B1-31, A2-1, A2-11) at 1847 Ma (MSWD = 36). Because all these fractions (except B1-31) correspond to rounded zircons with minimal core material, the 1844 Ma age is interpreted as the time of metamorphic zircon growth or a migmatization event, as suggested by the magmatic-like regular zoning of equant grains (pop. 2) and by their high U content. Older cores, however, have been recognized in rounded grains (pop. 2) from which $^{207}Pb/^{206}Pb$ ages of 1886–2087 Ma were obtained using the zircon evaporation technique (Kober 1987). Evaporation results from a brown, homogeneous grain (pop. 2) indicate a $^{207}Pb/^{206}Pb$ age of 1849 ± 5 Ma, in agreement with the conventional data.

Two fractions of rounded monazite have also been analyzed. One is concordant at 1857.1 ± 1.1 Ma, an age similar to the "needle" discordia, but a larger fraction (1.57% discordant, 14 grains) has a $^{207}Pb/^{206}Pb$ age of 1849 Ma. This age is intermediate between those defined from needles and rounded grains and suggests either a partial resetting or, more likely, a mixed population of two generations of monazites (ca. 1857 and ≤ 1844 Ma).

Hypersthene-bearing mobilizate vein (TK89 15)

This 50 cm wide by 20 m long vein was collected from the sharp contact between Tasiuyak gneiss and an enderbite body, close to the eastern margin of the TGC in the ASZ (Fig. 2). The vein follows the contact but intrudes and crosscuts some of the metamorphic layering of the Tasiuyak gneiss; it is therefore considered to closely constrain the age of syntectonic partial melting related to D_2 deformation within the ASZ.

Three fractions of single zircons from this sample have ages of 1844 ± 3.6 Ma (0.09% discordant), 1856 ± 3.6 (0.19% discordant), and 1859 Ma (0.39% discordant, Fig. 6B). The youngest grain, a rounded, colourless, short prism with a subhedral habit, may represent zircon crystallization during the emplacement of the vein and thus the age of the Abloviak shear zone. Older grains are clear, spherical, and colourless, with a discrete core component that is likely xenocrystic (Fig. 3J).

Tasiuyak leucogranite vein (ES89 G2)

This undeformed, east–west striking vein (5 m wide by ≥8 m long) of garnet-bearing pegmatitic leucogranite cuts the north–south sinistral shear foliation in the central part of the TGC (Fig. 2). The sample has an undeformed, coarse-grained assemblage of garnet, red biotite, plagioclase, microcline, subspherical quartz, and accessory minerals. It should provide a minimum

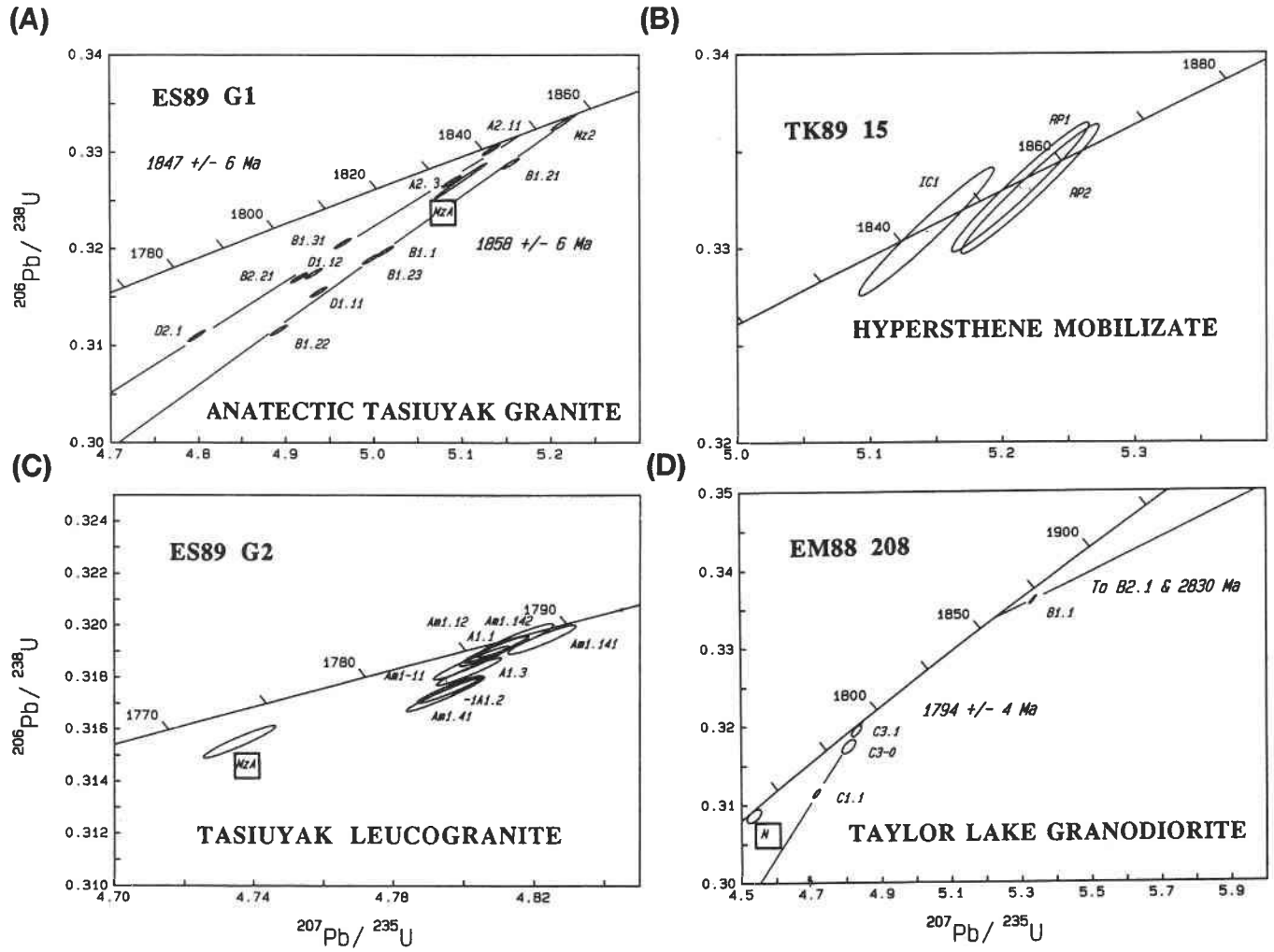

FIG. 6. Tasiuyak Gneiss complex $^{206}Pb/^{238}U$ vs. $^{207}Pb/^{235}U$ diagrams. (A) Anatectic Tasiuyak granite (ES89 G1). (B) Hypersthene-bearing mobilizate vein (TK89 15). (C) Tasiuyak leucogranite vein (ES89 G2). (D) Taylor Lake granodiorite (EM88 208). Error ellipses are 2σ.

age for the high-grade deformation (stage II) in the TGC.

Six populations of zircon have been observed in this sample (Table 1). SEM images show a regular, finely-zoned, sometimes sector-zoned, internal structure (Fig. 3K). In some cases, tiny residual "seeds" that may be cores or growth discontinuities are seen near the centre of the crystals. The whole zircon population is considered as having crystallized during a single event of crustal melting. Two populations have been selected for dating: seven fractions of multifaceted to rounded colourless grains (pop. 1), and one fraction of long, euhedral, colourless needles with irregular, bone-shaped cores (pop. 4) similar to those seen in sample ES89 G1.

Four core-free fractions (pop. 1) (Table 2) yield the youngest concordant to almost concordant ages (Fig. 6C), with a small but significant range in ages from 1789.9 ± 1.0 (A1-3, 0.56% discordant) to 1787.9 ± 1.1 Ma (Am1-12, 0.16% discordant). Ages of two fractions with tiny cores are in the same range: 1790.7 ± 1.3 (Am1-141, 0.23% discordant) to 1788.0 ± 1.5 Ma (Am1-142, 0.07% discordant). A fraction with obvious larger cores from pop. 1 (-1A1.2) and needles from pop. 4 (Am1-41) yield slightly older discordant $^{207}Pb/^{206}Pb$ ages of about 1792 Ma. These zircons appear to represent heterogeneous crystals formed during a protracted period of growth over a 1–6 Ma period.

Euhedral monazite yields a discordant (0.82%) $^{207}Pb/^{206}Pb$ age of 1780 Ma, corresponding to cooling of the vein to ca. 725°C.

Taylor Lake granodiorite (EM88 208)

This fine- to medium-grained, weakly foliated granodiorite sheet (20 m wide by ≥30 m long) at amphibolite facies, lies within and parallel to a north-northeast striking dextral shear zone that cuts the granulite-facies, D_2 structures in the Tasiuyak gneiss and associated enderbitic bodies in the North River domain. Such granodiorite sheets are commonly found within late mylonite- and pseudotachylite-bearing shear zones and are interpreted as having been emplaced during stage III (Van Kranendonk 1992*b*).

Three populations of zircon have been identified in this sample (Table 1): (*i*) Round-shaped brown zircon grains (pop. 1) with rims or "tails" of overgrowth material. SEM images show a sharp contrast between cores and multifaceted, subhedral to euhedral rims in these grains, which are interpreted as overgrowths (Figs. 3L, 3M). The euhedral shape of the core–overgrowth boundary is revealed by HF etching as a metamict zone in the core (Fig. 3M) and a white, discontinuous collar of partly altered zircon in the rims. This white material has also resorbed and filled cracks in the core (Fig. 3L). Cores,

which form a large proportion of the zircons in this sample, are clearly of xenocrystic origin, inherited either from the host rocks to the vein or from the source of the vein. Two fractions of abraded cores were analyzed: B1-1 has a minimum $^{207}Pb/^{206}Pb$ age of 1881 Ma (0.81% discordant), very close to the age of the oldest zircons found in the enderbite (sample EE89 023), which forms most of the country rock adjacent to the present sample; C1-1 is discordant, but aligned on a 1794 Ma discordia with euhedral zircons (Fig. 6D, see below). (*ii*) Short to flat prisms (pop. 2); the only analyzed fraction is discordant and yields a minimum $^{207}Pb/^{206}Pb$ age of 2416 Ma. (*iii*) Two fractions of euhedral, limpid, and colourless needles (pop. 3) yield ages of about 1795 Ma (C3-1; C3-0, the only unabraded fraction). This age is confirmed by a discordia at 1794 Ma (Fig. 6D), which includes C1-1 (a core from pop. 1). These euhedral zircons are interpreted to be of magmatic origin and therefore indicate the time of granodiorite emplacement at ca. 1794 Ma.

Euhedral monazite (0.5% discordant) gives a younger age of 1742 Ma, within the same age range (within errors) as the dated hornblende from the enderbite.

Western margin of the Nain Province

The five samples examined in this area are granitic to pegmatitic veins and stocks occurring near, or within, steep mylonitic zones (stage III) in the Foreland zone, where the Nain Province is deformed within the eastern edge of the ASZ (Fig. 2).

Pink deformed granite (RAL88 17)

This strongly deformed, medium-grained, equigranular biotite granite is one of several small (500 m − 1.5 km wide by 2−5 km long) stocks emplaced within reworked gneisses of the Nain Province to the west of the deformed Ramah Group (Van Kranendonk 1990, 1992*b*). The sampled body contains a subvertical foliation and a weak to strong down-dip lineation, which are interpreted as D_3 fabric elements. The granite is therefore interpreted as having been emplaced after stage II, but prior to, or during, stage III.

Three populations of zircons are present in the sample (Table 1). Clear glassy fragments of low-U euhedral zircon from pop. 1 (C1-1) define an age of 1805.8 ± 5.5 Ma, which just overlaps concordia (0.27% discordant, Fig. 7A). This age is consistent with two other fractions of euhedral grains (B1-1 with a large error ellipse; B2-1 a 1.47% discordant point with a $^{207}Pb/^{206}Pb$ age of 1805 Ma) and is interpreted as a magmatic age defining an older limit for the stage III orogenic activity. Two single discordant grains (pops. 1 and 3) with $^{207}Pb/^{206}Pb$ ages of 2560 and 2634 Ma indicate the presence of an inherited Archean component, whereas B1-2 ($^{207}Pb/^{206}Pb$ age 1865 Ma) has lesser inheritance.

Down-dip deformed pegmatite (EM89 121A)

This 1 m wide pegmatite was emplaced within an amphibolite- to greenschist-facies, subvertical D_3 shear zone separating the Ramah Group from reworked Archean rocks to the west. The vein crosscuts most of the mylonitic schistosity within the shear zone, but is strongly foliated with a down-dip stretching lineation, and is therefore interpreted as synkinematic with respect to stage III.

Six populations of zircon grains have been identified in this sample (Table 1). SEM images show a ubiquitous presence of cores, some of which have almost no contrast with thin overgrowths (Fig. 3N); other cores are slightly metamict. SEM observations also confirm that synneusis structures seen in the grains are related to the overgrowth stage, probably corresponding to emplacement of the pegmatite.

Overgrowths from most zircons were impossible to separate, except for pop. 6, which consists of large broken tips. Isotopic results show that the slightly metamict cores are all inherited; a reference line with poorly defined upper (ca. 3275 Ma) and lower (1824 ± 21 Ma) intercepts (Fig. 7*b*) suggests several sources of inheritance, from ca. 2.6 to 3.3 Ga. Fractions of separated tips fall on the same reference line. This may indicate that the overgrowths are actually part of xenocrysts and possibly represent growth during an Archean metamorphic event. An almost concordant (0.14% discordant) fraction of euhedral monazite yields an age of 1773.1 ± 1.1 Ma, which likely represents the emplacement age of the pegmatite.

Ramah granite (ES89 22a)

This diffuse, schlieric, microcline−garnet−biotite−sillimanite granite is one of several small, meter- to decameter-sized, irregular-shaped bodies that crosscut folded metasediments of the Ramah Group but are themselves strongly foliated. The sample is medium-grained with incipient mylonitic textures. The emplacement age of this granitoid rock with respect to the early phases of deformation is unknown, but it predates stage III deformation.

Four diamagnetic zircon fractions were analyzed. Two fractions of very clear fragments of almost euhedral zircons, representing overgrowths (-1B1-1 and -1B1-2, pop. 1), are collinear with a fraction of core fragments (-1B2-3, pop. 2) and define a discordia with a lower intercept at 1794 ± 12 Ma (MSWD = 5) and an upper intercept at ca. 2995 Ma (Fig. 7C). A fourth fraction of two abraded cores from short bipyramids yields an older apparent age (-1B3-1, pop. 3). Because of significant inheritance in all fractions, these ages are interpreted as approximating the age of granite emplacement and the age of Archean sources, respectively. Euhedral monazite gives an age of 1739 Ma (0.69% discordant), similar to the youngest cooling ages found in the LLC (hornblende from the enderbite) and in the TGC (monazite of the Taylor Lake granodiorite).

Ramah sillimanite granite mylonite (ES89 22b)

This sillimanite-bearing granite vein (20 cm wide by 5 m long) from the eastern edge of the Ramah Group is strongly deformed, with a down-dip lineation defined by metamorphic biotite, muscovite, and fibrous quartz. Sillimanite inclusions in plagioclase are interpreted to be magmatic remnants. This rock type has been observed in both deformed and undeformed states in the same shear zone, suggesting a syntectonic emplacement during stage III uplift.

Three populations of zircons were observed in the nonmagnetic fraction (Table 1). SEM images show a regular euhedral zoning surrounding small anhedral, often metamict cores (Fig. 3O). Analyses were carried out on separated tips of pop. 2 and broken fragments probably derived from short euhedral prisms with, or devoid of, cores from both pops. 1 and 2. Two weakly discordant fractions yield ages of 1785 (A3-1, 0.46% discordant) and 1787 Ma (A3-2, 0.88% discordant; Fig. 7C). Two other, more discordant fractions of pale brown tips have inheritance ($^{207}Pb/^{206}Pb$ ages of 1802 and 1998 Ma). Based on magmatic-like zoning, the average zircon age from the two almost concordant fractions (1786 Ma) is interpreted to represent the emplacement age of this granite, probably synkinematic with the uplift. This interpretation is confirmed by reversely discordant euhedral monazite (−0.39% discordant), with a $^{207}Pb/^{206}Pb$ age of 1781.6 ± 1.0 Ma and

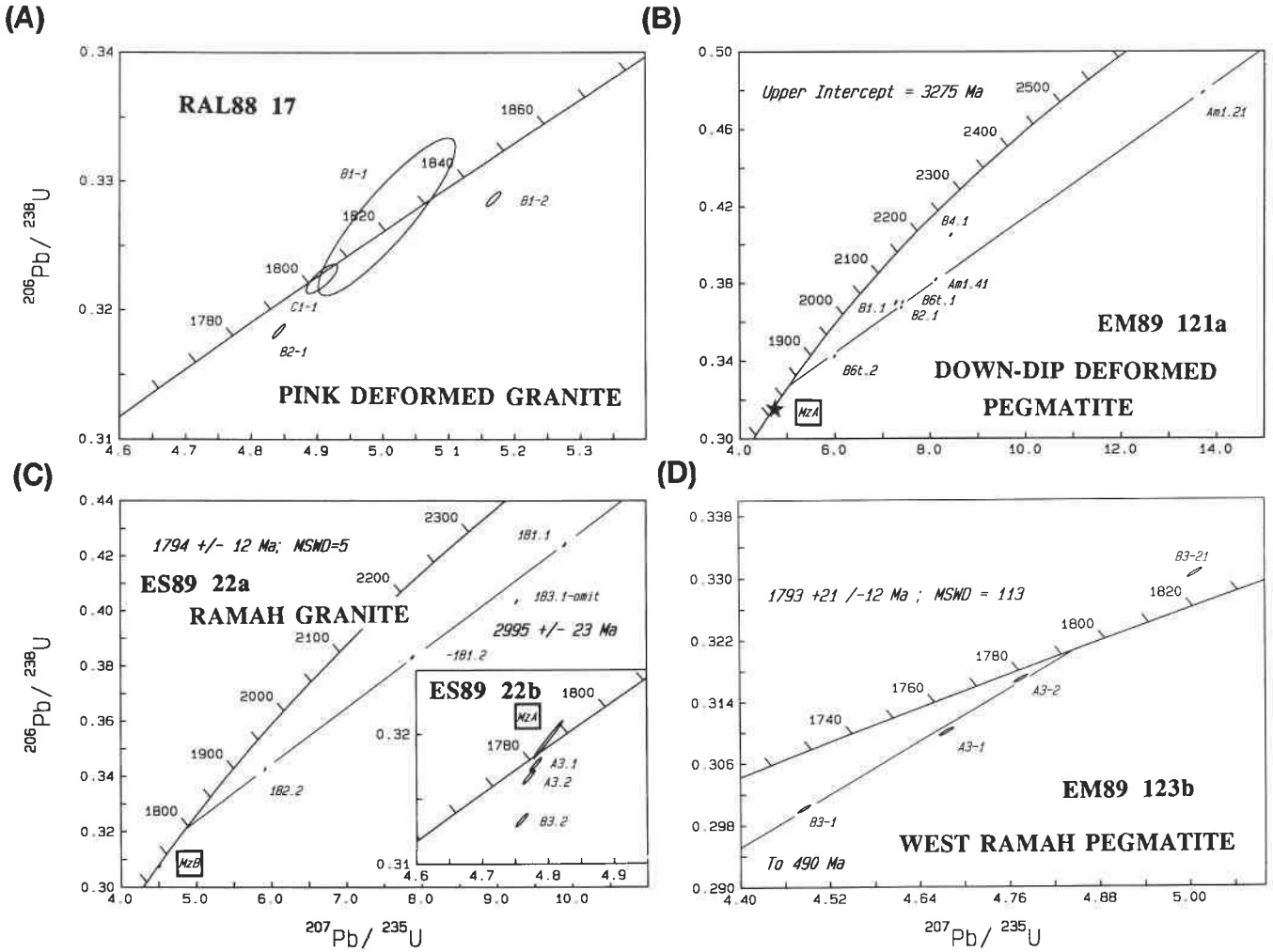

FIG. 7. $^{206}Pb/^{238}U$ vs. $^{207}Pb/^{235}U$ diagrams of samples from the Foreland zone. (A) Pink deformed granite (RAL88 17). (B) Down-dip deformed pegmatite (ES89 121a). (C) Ramah granite (ES89 22a); Ramah sillimanite granite mylonite (ES89 22b) in insert. (D) West Ramah pegmatite (EM89 123b). Error ellipses are 2σ.

a $^{207}Pb/^{235}U$ age of 1784.1 ± 4 Ma.

West Ramah pegmatite (EM89 123B)

This 1m wide, amphibolite-facies pegmatite vein from the eastern margin of the Abloviak shear zone (Fig. 2) strikes north–northwest, is openly folded, and contains a weak foliation subparallel to stage II structures. The low-grade vein is interpreted as either late tectonic to stage II or as syntectonic with stage III but removed from the bulk of the strain related to this event.

Three zircon populations have been observed (Table 1), but the only analyzed fractions are from large brown, euhedral grains and fragments (pop. 3). Other populations are either very scarce (pop. 1) or of poor quality (pop. 2). SEM images show that the zircons (pop. 3) are highly metamict with transparent outer zones, which may represent nonmetamict, U-poor overgrowths. A fraction of tiny clear fragments (A3-2), obtained by a short abrasion of metamict grains (the outer shell in Fig. 3P), yield the most concordant point with an age of 1787 Ma (0.78% discordant). Two other fractions of clear tips devoid of any core remnants fall on a similar 1.79 Ga discordia (upper intercept at 1793^{+21}_{-12} Ma, Fig. 7D). A third fraction (B3-21) lies above concordia (−2.8% discordant) on the same discordia line. This imprecise age of the pegmatite is similar to that of the Ramah sillimanite granite and dates the uplift related deformation (stage III) in the Foreland zone.

Discussion and conclusions

In the high-grade, complexly deformed rocks of the Torngat Orogen, interpretation of zircon U–Pb data and derived discordia lines are often difficult. Measured ages do not always correlate with zircon morphology and observed growth history, as, for example, in the apparent equilibration between cores and overgrowths in samples EM89 019 and ES89 G1. For this reason we have chosen to give more credit to concordant data, rather than discordia regression ages.

Chronology of events

U–Pb ages from across the Torngat Orogen in the North River map area are presented in Table 3, and a sketch of the tectonic evolution is shown in Fig. 8. The data fall into several age groups, some of which are geographically restricted to a particular structural zone. Archean to Early Proterozoic inherited zircons are found in small quantities in many of the samples and confirm an Archean crustal age for at least some of the southeastern Rae Province and for the strip of gneisses immediately west of the Ramah Group. In the following section, the

TABLE 3. U–Pb ages from across the Torngat Orogen

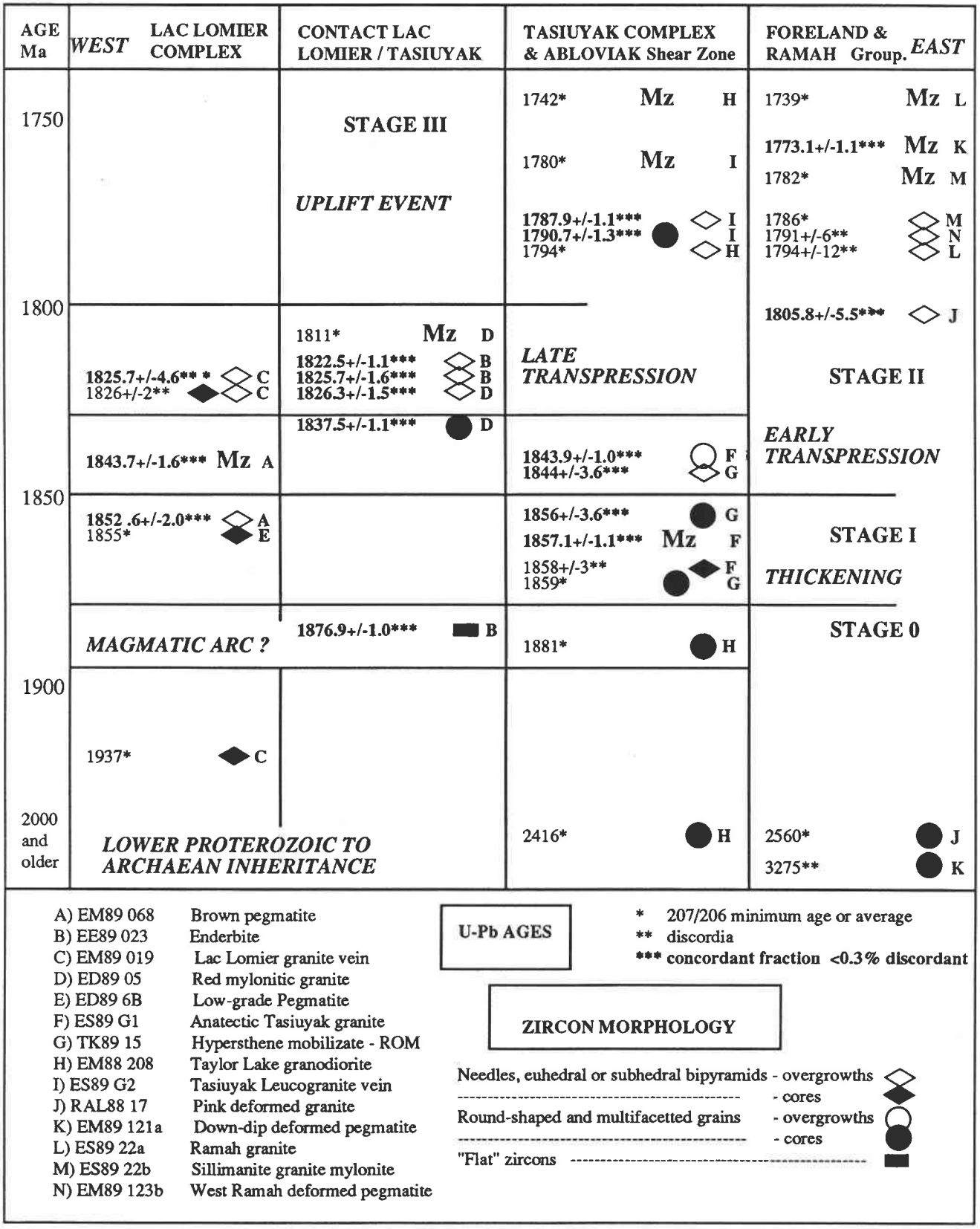

geochronology is used to constrain the established structural sequence developed by Van Kranendonk and Ermanovics (1990) (see also Van Kranendonk 1990, 1992*b*; Ermanovics and Van Kranendonk 1990).

Pretectonic arc magmatism (stage 0), ca. 1880 Ma

Limited age data exists from the Early Proterozoic enderbite–charnockite suite found across the TGC and LLC. The pretectonic character and calc-alkaline composition of the suite

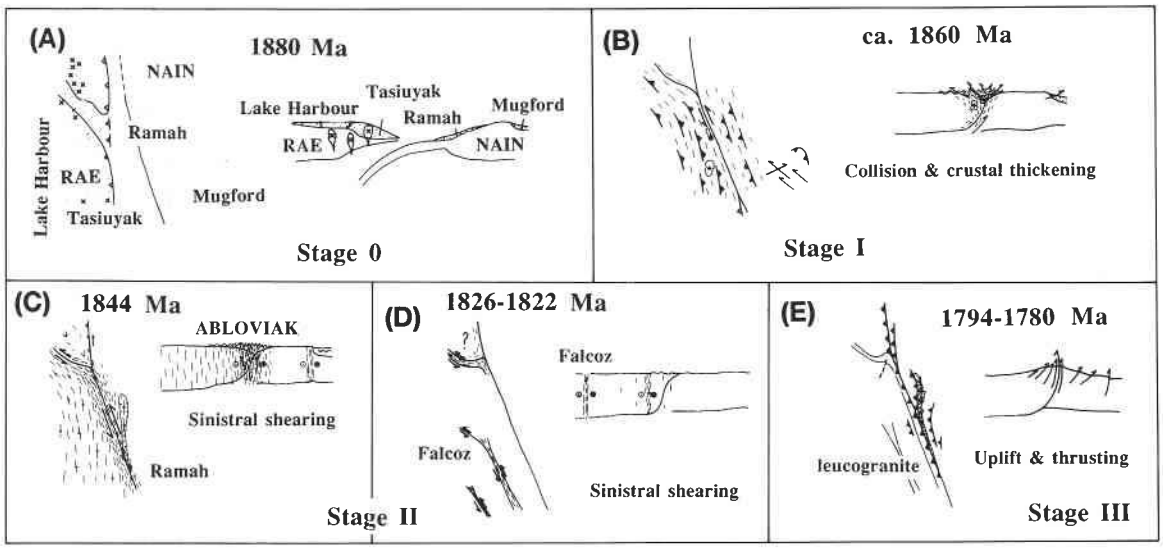

FIG. 8. Schematic diagram of the geotectonic evolution of the Torngat Orogen after Van Kranendonk (1992*b*).

(cf. Iyer 1980; Schaumann 1987) suggests that it represents a magmatic arc, interpreted to have developed as a result of westward subduction under the eastern margin of the southeastern Rae Province (Van Kranendonk 1990, 1992*b*; Fig. 8A). The 1876.9 ± 1.1 Ma age of the oldest zircons of the enderbite is interpreted to date the time of arc magmatism in the Torngat Orogen.

Stage I crustal thickening, ca. 1860 Ma

Stage I deformation is associated with crustal thickening as a result of Nain–Rae continent–continent collision across the Tornat Orogen (Van Kranendonk 1990, 1992*b*). The age of this event has been determined as ca. 1860 Ma from zircon cores and xenocrysts, monazite xenocrysts, and (or) concordant new zircon from 5 samples across the orogen, including the following: (*i*) In the LLC, zircons from a granulite-facies pegmatite (EM89 068) at 1852.7 ± 1.6 Ma and from a lower grade pegmatite (ED89 6b) at ca. 1855 Ma. (*ii*) In the TGC, an anatectic granite (ES89 G1) yields ages of 1858 Ma and 1857.1 ± 1.1 Ma from zircon cores and rounded monazite, respectively. Zircon xenocrysts from a syntectonic mobilizate vein (TK89 15) were dated as 1856 ± 3.6 and 1859 ± 3.6 Ma. (*iii*) Unpublished zircon data (J.C. Roddick and M. Van Kranendonk) from the eastern margin of the Pistolet Bay fold structure in the Nain Province, 30 km east of the eastern margin of the Torngat Orogen (Van Kranendonk and Helmstaedt 1990), show almost concordant ages of 1858 and 1855 Ma on two single grains, related to growth of new zircon during Early Proterozoic amphibolite to greenschist-facies alteration of Archean granulite-facies assemblages (Van Kranendonk 1992*b*).

These results provide a common age of between ca. 1859 and 1853 Ma for the onset of Early Proterozoic deformation and metamorphism across the Nain–Rae province boundary, interpreted as the result from the initial collision of the Nain and Rae provinces (stage I, Fig. 8B). Similar ages from the Nain – Strange Lake corridor southwest of the map area (Ryan et al. 1991) show that this event was widespread in the Torngat Orogen.

Stage II sinistral transpression, ca. 1845–1820 Ma

Granulite-facies metamorphism and structural features indicative of sinistral transpressional shear occur across the Torngat Orogen, with strain intensity decreasing from east to west (Van Kranendonk 1990, 1992*b*; Van Kranendonk and Ermanovics 1990). Crystallization of zircon, mostly as large overgrowths on preexisting grains, occurred during this event in most of the metamorphic assemblages. Three peak ages, corresponding to discrete events, have been determined:

(1) The main high-grade transcurrent regime has been dated at ca. 1844 Ma in the high-strain rocks of the Abloviak shear zone (TK89 15, 1844 ± 3.6 Ma), in an anatectic granite emplaced in the Tasiuyak gneiss (ES89 G1, 1843.9 ± 1.0 Ma), and in sample EM89 068 from the LLC, where monazite indicates an age of 1843.7 ± 1.6 Ma for the high-grade shearing. Thus the 1844 Ma event occurred throughout the orogen in the map area. We interpret this age as the initiation of stage II sinistral transpressive shearing under granulite-facies conditions and the time of formation of the Abloviak shear zone (Fig. 8C).

(2) Magmatic zircon cores from a mylonitic granitoid gneiss emplaced along the sheared boundary between LLC and TGC (ED89 05), dated as 1837.5 ± 1.1 Ma, apparently represents a discrete intrusive event in the evolution of the Torngat Orogen.

(3) An age event at 1826–1822 Ma is restricted to the North River domain and is defined by new zircon crystallization in some granulite-facies rocks (EE89 023), by magmatic overgrowths of inherited zircon cores in a granite vein emplaced into amphibolite-facies conditions (EM89 019), and by metamorphic zircon overgrowths in a granitoid rock sheared at amphibolite facies (ED89 05). The amphibolite-facies metamorphic assemblage of the latter samples suggests continued sinistral shearing from granulite to amphibolite facies, probably representing the end stages of a progressive stage II transcurrent regime. The absence of this event in samples of the Abloviak shear zone (1844 Ma) may indicate a westerly migration of deformation in time. Alternatively, the absence of this event also in some samples from the LLC suggests that the younger derformation was localized within discrete, possibly anastomosing shears. The undated, granulite- to amphibolite-facies Falcoz shear zone that cuts the north–south striking fabric elements of the North River domain in the southwestern corner of the map area, may also have formed at this time (Fig. 8D).

Post-stage II granites, 1806 Ma

Several small granitic stocks occur within reworked Nain gneisses along the Abloviak shear zone – Foreland zone boundary, where they are deformed within late, retrograde, uplift-related shear zones (stage III). One of these has been dated at 1805.8 ± 5.5 Ma and therefore provides a minimum age for the end of stage II deformation and a maximum age constraint for the onset of stage III.

Stage III uplift, 1795–1740 Ma

Undeformed to mylonitized, syn-stage III granitic and pegmatitic veins have been used to decipher the late history of the orogen along its eastern margin. Many zircons in the analyzed samples are inherited but younger zircon ages range from 1794 to 1785 Ma, including the following: (*i*) Magmatic overgrowths and euhedral zircons from the Taylor Lake granodiorite (EM88 208), dated at 1794 Ma. Poorly defined discordia from the Ramah granite and the West Ramah pegmatite yield the same age. (*ii*) In the TGC, the post-D_2, undeformed leucogranite pegmatite (ES89 G2) yields a zircon age of 1787.9 ± 1.1 Ma, interpreted as the emplacement age, with slightly older cores, up to 1792 Ma. Such an age pattern may correspond to protracted decompression melting related to uplift (Zeitler and Page Chamberlain 1991). (*iii*) In the Foreland zone, the pegmatite (EM89 123b) from west of the Ramah Group yields a reasonably good zircon age of 1787 Ma. The down-dip lineated sillimanite-granite (ES89 22b) from the eastern margin of the Ramah Group yields similar, almost concordant ages for euhedral magmatic zircon (1785 and 1787 Ma) and monazite (1784.1 ± 4 $^{207}Pb/^{235}U$ age).

Monazite data, where available, are considered to give reliable estimates of the emplacement ages of the veins. In two cases, the age difference between zircon and monazite is similar (for ES89 G2 undeformed pegmatite and ES89 22b Ramah sillimanite granite zircon is 1787–1788 Ma and monazite is 1780 Ma), suggesting a direct relationship between age and closure temperatures of the mineral phases. The concordant monazite age of 1773.1 ± 1.1 Ma from a down-dip lineated pegmatite (sample EM89 121a; in which all zircons are inherited) is the best estimate of the time of emplacement and stage III uplift, and is identical to the 1774 Ma age of post-tectonic granite intrusions within the Nain Province (Emslie and Loveridge 1992). Similar $^{40}Ar/^{39}Ar$ hornblende ages have also been established for the Saglek Fjord area farther north (Mengel et al. 1991).

Younger, discordant monazite ages of ca. 1740 Ma were obtained from granitic veins in the Foreland zone (sample ES89 22a) and the TGC (EM88 208); they are similar to a $^{40}Ar/^{39}Ar$ age of hornblende (enderbite EE89 023) and to hornblende ages determined further north in the equivalent of our Foreland zone (Mengel et al. 1991). If these monazite dates are interpreted as minimum ages close to magmatic emplacement ages, this would imply that several magmatic pulses at ca. 1794, 1788, 1780, 1773, and 1740 Ma were associated with episodic uplift movement along the Abloviak shear zone – Foreland zone boundary. Alternatively, different parts of the orogen may have cooled through the closure temperature of monazite at different times, thus accounting for the scatter in monazite ages.

Regional significance for the tectonic assembly of northeastern Laurentia

The age groups defined within the study area (Table 3) are broadly similar to those from across northeastern Laurentia and have significant implications for the Early Proterozoic tectonic assembly of this region. Firstly, the interpreted age of enderbitic magmatism and therefore of westward subduction in the southeastern Rae Province, at ca. 1880 Ma, is similar to that in the Cumberland batholithic complex (Jackson et al. 1990) and to foredeep magmatism or transtensional basin development (marking the onset of orogeny) in the New Quebec Orogen (Machado et al. 1989). This confirms one element of the model proposed by Hoffman (1990), in that mafic magmatism in the New Quebec Orogen was contemporaneous with subduction beneath the northeastern margin of the southeastern arm of the Rae Province.

Most important, however, is the conclusion that Nain–Rae collision occurred at ca. 1860 Ma across the Torngat Orogen, approximately 35–40 Ma *prior* to the collisional orogeny across the Ungava Orogen, dated as ≤1826 Ma (Parrish 1989; St-Onge et al. 1992; Lucas et al. 1992), and approximately 15–20 Ma before that across the New Quebec Orogen (Perreault et al. 1988). This data disproves a critical element of Hoffman's (1990) model, in that northward indentation of the Superior Province into a hinterland of Rae Province is not a viable mechanism to extrude the southeastern Rae Province or to form the ancestral Baffin basin (Cumberland batholithic complex; Van Kranendonk 1992*a*). Instead, the data show that the southeastern Rae Province must have been separate from its more northerly parent prior to Nain – southeastern Rae collision and Superior indentation.

Subsequent to Nain–Rae collision at ca. 1860, deformation events between ca. 1845–1805 Ma in the Torngat Orogen fall within similar age groupings as data from across northeastern Laurentia (e.g., Schärer et al. 1988, Perreault et al. 1988), thereby confirming a coeval evolution of this region over this time interval (Hoffman 1988, 1990). The time between 1790–1740 Ma was one of thrusting and retrograde metamorphism in both the New Quebec (Perreault et al. 1988) and Torngat orogens (this study, Mengel et al. 1991). The direction of thrusting was opposite in the two orogens, reflecting the late rise of the ductile southeastern Rae Province between its rigid Superior and Nain province neighbours (Van Kranendonk 1992*a*). In both orogens, the end of orogenic activity is marked by the emplacement of late granites at ca. 1775–1774 Ma (Perreault et al. 1988; Emslie and Loveridge 1992), but uplift in the Torngat Orogen may have continued until 1740 Ma.

Acknowledgments

J.M.B. is grateful to the Centre national de la recherche scientifique (CNRS), who permitted sabbatical leave in 1989–1990 during which most of this study was carried out at the Geological Survey of Canada, Ottawa, and for a grant to complete this paper in Ottawa (CNRS and Direction de la coopération technique, Affaires étrangères). S. Hanmer is thanked for the initial impetus of the joint U–Pb zircon dating – structural project and for providing some key samples. We are indebted to Tom Krogh for providing sample TK89 15, which J.M.B. analyzed at the Royal Ontario Museum, Toronto; Kim Davis is thanked for her help in processing the sample. We thank also the staff of the Geochronology Lab in Ottawa for help and discussions at all stages of this work. Thanks also to M. Villeneuve (Ottawa) and A. Kohler (Nancy) for the SEM images. C. Pin and M. Wiedenbeck kindly helped to improve early drafts of this paper. A critical review by R. Parrish and editorial reviews by B. Ryan and C. Gariépy were greatly appreciated.

Bertrand, J.M., Van Kranendonk, M.J., Hanmer, S., Roddick, J.C., and Ermanovics, I. 1990. Structural and metamorphic geochronology of the Torngat Orogen in the North River – Nutak transect area, Labrador. Geoscience Canada, **17**: 297–301.

Black, L.P., Williams, I.S., and Compston, W. 1986. Four zircon ages from one rock: the history of a 3930 Ma-old granulite from Mount Stones, Enderby Land, Antartica. Contributions to Mineralogy and Petrology, **94**: 427–437.

Emslie, R.F., and Loveridge, W.D., 1992. Fluorite-bearing Early and Middle Proterozoic granites, Okak Bay area, Labrador: geochronology, geochemistry and petrogenesis. Lithos, **28**: 87–109.

Ermanovics, I., and Van Kranendonk, M.J. 1990. The Nutak – North River transect of Nain and Churchill provinces: the Torngat Orogen. Geoscience Canada, **17**: 279–283.

Ermanovics, I., Van Kranendonk, M., Corriveau, L., Mengel, F., Bridgwater, D., and Sherlock, R. 1989. The boundary zone of the Nain–Churchill provinces in the North River – Nutak map areas, Labrador. Geological Survey of Canada, Paper 89-1C, 385–394.

Hoffman, P.F. 1988. United Plates of North America, the birth of a craton: Early Proterozoic assembly and growth of Laurentia. Annual Reviews of Earth and Planetary Sciences, **16**: 543–603.

Hoffman, P.F. 1990. Dynamics of the tectonic assembly of northeast Laurentia in geon 18 (1.9–1.8 Ga). Geoscience Canada, **17**: 222–226.

Iyer, G.V.A. 1980. Petrology, mineralogy and geochemistry of granulites of the Ford River and North River belts of northern Labrador, Canadian Shield. Geological Survey of Canada, Paper 80-9.

Jackson, G.D., and Taylor, F.C. 1972. Correlation of major Aphebian rock units in the northeastern Canadian Shield. Canadian Journal of Earth Sciences, **9**: 1650–1669.

Jackson, G.D., Hunt, P.A., Loveridge, W.D., and Parrish, R.R. 1990. Reconnaissance geochronology of Baffin Island, N.W.T. *In* Radiogenic age and isotopic studies: Report 3. Geological Survey of Canada, Paper 89-2, pp. 123–148.

Kober, B. 1987. Single-zircon evaporation combined with Pb* emitter bedding for $^{207}Pb/^{206}Pb$-age investigations using thermal ion mass spectrometry, and implications to zirconology. Contributions to Mineralogy and Petrology, **96**: 63–71.

Krogh, T.E. 1982. Improved accuracy of U–Pb zircon ages by the creation of more concordant systems using an air abrasion technique. Geochimica et Cosmochimica Acta, **46**: 637–649.

Krogh, T.E. 1990. Geochronology report. Geological Survey Branch, Newfoundland Department of Mines and Energy, Open File 14D/40.

Krogh, T.E., and Heaman, L.M. 1989. Report on U–Pb results for the 1988/89 Labrador geochronology contract. Unpublished results on file with Mineral Development Division, Newfoundland Department of Mines and Energy, St John's.

Lucas, S.B., St-Onge, M.R., Parrish, R.R., and Dunphy, J.M. 1992. Long-lived continent–ocean interaction in the Early, Proterozoic Ungava Orogen, northern Quebec, Canada. Geology, **20**: 113–116.

Machado, N., Goulet, N., and Gariépy, C. 1989. U–Pb geochronology of reactivated Archean basement and of Hudsonian metamorphism in the northern Labrador Trough. Canadian Journal of Earth Sciences, **26**: 1–15.

Mengel, F., and Rivers, T. 1989. Thermotectonic evolution of the Proterozoic and reworked terranes along the Nain/Churchill boundary in the Saglek area, northern Labrador. *In* Evolution of metamorphic belts. *Edited by* J.S. Daly, R.A. Cliff, and B.W.D. Yardley. Geological Society, Special Publication (London), No. 43, pp. 319–324.

Mengel, F., and Rivers, T. 1991. Decompression reactions and P–T conditions in high-grade rocks, northern Labrador: P–T–t paths from individual samples and implications for Early Proterozoic tectonic evolution. Journal of Petrology, **32**: 139–167.

Mengel, F., Rivers, T., and Reynolds, P. 1991. Lithotectonic elements and tectonic evolution of Torngat Orogen, Saglek Fiord, northern Labrador. Canadian Journal of Earth Sciences, **28**: 1407–1423.

Parrish, R.R. 1989. U–Pb geochronology of the Cape Smith Belt and Sugluk block, northern Quebec. Geoscience Canada, **16**: 126–130.

Parrish, R.R. 1990. U–Pb dating of monazite and its application to geological problems. Canadian Journal of Earth Sciences, **27**: 1431–1450.

Parrish, R.R., Roddick, J.C., Loveridge, W.D., and Sullivan, R.W. 1987. Uranium–lead analytical techniques at the Geochronology Laboratory, Geological Survey of Canada. *In* Radiogenic age and isotopic studies: Report 1. Geological Survey of Canada, Paper 87-2, pp. 3–7.

Perreault, S., and Hynes, A. 1990. Tectonic evolution of the Kuujjuaq terrane, New Quebec Orogen. Geoscience Canada, **17**: 238–240.

Perreault, S., Hynes, A., and Machado, N. 1988. Timing in the tectonic evolution of the NE segment of the Labrador Trough, Kuujjuaq, northern Quebec. Geological Association of Canada, Program with Abstracts, **13**: 97–98.

Pupin, J.P. 1980. Zircon and granite petrology. Contributions to Mineralogy and Petrology, **73**: 207–220.

Roddick, J.C. 1987. Generalized numerical error analysis with applications to geochronology and thermodynamics. Geochimica et Cosmochimica Acta, **51**: 2129–2135.

Roddick, J.C. 1990. $^{40}Ar/^{39}Ar$ evidence for the age of the New Quebec Crater, northern Quebec. *In* Radiogenic age and isotopic studies: Report 3. Geological Survey of Canada, Paper 89-2, pp. 7–16.

Roddick, J.C., Loveridge, W.D., and Parrish, R.R. 1987. Precise U/Pb dating of zircon at the sub-nanogram Pb level. Isotope Geoscience, **66**: 111–121.

Ryan, B. 1990. Does the Labrador–Quebec border area of the Rae (Churchill) Province preserve vestiges of an Archean history? Geoscience Canada, **17**: 255–259.

Ryan, B., Krogh, T.E., Heaman, L., Schärer, U., Philppe, S., and Oliver, G. 1991. On recent geochronological studies in the Nain province, Churchill province and Nain plutonic suite, north-central Labrador. *In* Current Research. Newfoundland Department of Mines and Energy, Geological Survey Branch, Report 91-1, pp. 257–261.

Schärer, U., Krogh, T.E., Wardle, R.J., Ryan, B., and Gandhi, S.S. 1988. U–Pb ages of early and middle Proterozoic volcanism and metamorphism in the Makkovik Orogen, Labrador. Canadian Journal of Earth Sciences, **25**: 1098–1107.

Schaumann, S. 1987. Hebron Fjord Omradet: en petrologisk og geokemisk beskrivelse a bjergarter fra en shear zone. Upubliceret Cand-Scient. speciale, Aarhus Universitet.

Stacey, J.S., and Kramers, J.D. 1975. Approximation of terrestrial lead isotope evolution by a two-stage model. Earth and Planetary Science Letters, **26**: 207–221.

Steiger, R.H., and Jäger, E. 1977. Subcommission on geochronology: conventions on the use of decay constants in geo- and cosmochronology. Earth and Planetary Science Letters, **36:** 359–362.

St-Onge, M.R., Lucas, S.B., and Parrish, R.R. 1992. Terrane accretion in the internal zone of the Ungava orogen, northern Quebec. Part I: Tectonostratigraphic assemblages and their tectonic implications. Canadian Journal of Earth Sciences, **29**: 746–764.

Taylor, F.C. 1979. Reconnaissance geology of a part of the Precambrian Shield, northeastern Quebec, northern Labrador and Northwest Territories. Geological Survey of Canada, Memoir 393.

Van Kranendonk, M.J. 1990. Structural history and geotectonic evolution of the eastern Torngat Orogen in the North River map area, Labrador. *In* Current research, part C. Geological Survey of Canada, Paper 90-1C, pp. 81–96.

Van Kranendonk, M.J. 1992*a*. New insights on the tectonic assembly of northeastern Laurentia from 1.9–1.75 Ga. Eos, Transactions, American Geophysical union, **73**: 333.

Van Kranendonk, M.J. 1992*b*. Archean and Early Proterozoic geology of a transect across the Nain Province and Torngat Orogen in the North River – Nutak map area, northern Labrador, Canada. Ph.D. thesis, Queen's University, Kingston, Ont.

Van Kranendonk, M.J., and Ermanovics, I. 1990. Hudsonian deformation history of the eastern Torngat Orogen in the North River map area, Labrador: evidence for oblique collision along the Rae–Nain boundary zone, Geoscience Canada, **17**: 283–288.

Van Kranendonk, M.J. and Helmstaedt, H. 1990. Late Archean geologic history of the Nain Province, North River – Nutak map area, Labrador, and its tectonic significance. Geoscience Canada, **17**: 231–237.

Wanless, R.K., and Loveridge, W.D. 1978. Rubidium–Strontium isotopic age studies, Report 2 (Canadian Shield). Geological Survey of Canada, Paper 77-14.

Wardle, R.J. 1983. Nain–Churchill Province cross-section, Nachvak Fiord, northern Labrador. *In* Current research. Newfoundland Department of Mines and Energy, Report 83-1, pp. 68–89.

Wardle, R.J., Ryan, A.B., Nunn, G.A.C., and Mengel, F.C. 1990. Labrador segment of the Trans-Hudson Orogen: crustal development through oblique convergence and collision. *In* The Trans-Hudson Orogen of North America. *Edited by* J.F. Lewry and M.R. Stauffer. Geological Association of Canada, Special Paper 37, pp. 353–369.

York, D. 1969. Least squares fitting of a straight line with correlated errors. Earth and Planetary Science Letters, **5**: 320–324.

Zeitler, P.K., and Page Chamberlain, C. 1991. Petrogenetic and tectonic significance of young leucogranites from the nortwestern Himalaya, Pakistan. Tectonics, **10**: 729–741.

This article has been cited by:

1. R. A. Mason, R. K. Mitchell, R. Wirth, A. Indares. 2014. An electron-optical study of melt-related microstructures in granulite facies rocks from the Torngat Orogen. *Journal of Metamorphic Geology* **32**:10.1111/jmg.2014.32.issue-6, 557-574. [CrossRef]
2. R. K. Mitchell, A. Indares, B. Ryan. 2014. High to ultrahigh temperature contact metamorphism and dry partial melting of the Tasiuyak paragneiss, Northern Labrador. *Journal of Metamorphic Geology* **32**:10.1111/jmg.2014.32.issue-6, 535-555. [CrossRef]
3. J. Conliffe, D.H.C. Wilton, N.J.F. Blamey, S.M. Archibald. 2013. Paleoproterozoic Mississippi Valley Type Pb–Zn mineralization in the Ramah Group, Northern Labrador: Stable isotope, fluid inclusion and quantitative fluid inclusion gas analyses. *Chemical Geology* **362**, 211-223. [CrossRef]
4. E. D. KELLY, W. D. CARLSON, J. N. CONNELLY. 2011. Implications of garnet resorption for the Lu-Hf garnet geochronometer: an example from the contact aureole of the Makhavinekh Lake Pluton, Labrador. *Journal of Metamorphic Geology* **29**, 901-916. [CrossRef]
5. W. D. CARLSON. 2010. Dependence of reaction kinetics on H2O activity as inferred from rates of intergranular diffusion of aluminium. *Journal of Metamorphic Geology* no-no. [CrossRef]
6. Tanya Tettelaar, Aphrodite Indares. 2007. Granulite-facies regional and contact metamorphism of the Tasiuyak paragneiss, northern Labrador: textural evolution and interpretation. *Canadian Journal of Earth Sciences* **44**:10, 1413-1437. [Abstract] [PDF] [PDF Plus]
7. Christopher R.M. McFarlane, James N. Connelly, William D. Carlson. 2006. Contrasting response of monazite and zircon to a high-T thermal overprint. *Lithos* **88**, 135-149. [CrossRef]
8. Christopher R.M. McFarlane, James N. Connelly, William D. Carlson. 2005. Intracrystalline redistribution of Pb in zircon during high-temperature contact metamorphism. *Chemical Geology* **217**, 1-28. [CrossRef]
9. Alana M. Rawlings-Hinchey, Paul J. Sylvester, John S. Myers, Greg R. Dunning, Jan Kosler. 2003. Paleoproterozoic crustal genesis: calc-alkaline magmatism of the Torngat Orogen, Voisey's Bay area, Labrador. *Precambrian Research* **125**, 55-85. [CrossRef]
10. Guochun Zhao, Peter A Cawood, Simon A Wilde, Min Sun. 2002. Review of global 2.1–1.8 Ga orogens: implications for a pre-Rodinia supercontinent. *Earth-Science Reviews* **59**, 125-162. [CrossRef]
11. Anne-Magali Seydoux-Guillaume, Jean-Louis Paquette, Michael Wiedenbeck, Jean-Marc Montel, Wilhelm Heinrich. 2002. Experimental resetting of the U–Th–Pb systems in monazite. *Chemical Geology* **191**, 165-181. [CrossRef]
12. Richard J Wardle, Donald T James, David J Scott, Jeremy Hall. 2002. The southeastern Churchill Province: synthesis of a Paleoproterozoic transpressional orogen. *Canadian Journal of Earth Sciences* **39**:5, 639-663. [Abstract] [PDF] [PDF Plus]
13. Jeroen A.M van Gool, James N Connelly, Mogens Marker, Flemming C Mengel. 2002. The Nagssugtoqidian Orogen of West Greenland: tectonic evolution and regional correlations from a West Greenland perspective. *Canadian Journal of Earth Sciences* **39**:5, 665-686. [Abstract] [PDF] [PDF Plus]
14. J. N. Connelly, F. C. Mengel. 2000. Evolution of Archean components in the Paleoproterozoic Nagssugtoqidian orogen, West Greenland. *Geological Society of America Bulletin* **112**, 747-763. [CrossRef]
15. Stéphane Digonnet, Normand Goulet, James Bourne, Ross Stevenson, Doug Archibald. 2000. Petrology of the Abloviak Aillikite dykes, New Québec: evidence for a Cambrian diamondiferous alkaline province in northeastern North America. *Canadian Journal of Earth Sciences* **37**:4, 517-533. [Abstract] [PDF] [PDF Plus]
16. Thomas Funck, Keith E. Louden, Ian D. Reid. 2000. Wide-angle seismic imaging of a Mesoproterozoic anorthosite complex: The Nain Plutonic Suite in Labrador, Canada. *Journal of Geophysical Research* **105**, 25693. [CrossRef]
17. Thomas Funck, Keith E. Louden, Richard J. Wardle, Jeremy Hall, James W. Hobro, Matthew H. Salisbury, Angelina M. Muzzatti. 2000. Three-dimensional structure of the Torngat Orogen (NE Canada) from active seismic tomography. *Journal of Geophysical Research* **105**, 23403. [CrossRef]
18. Stephen J Piercey, Derek HC Wilton. 1999. Geochemical and radiogenic isotope (Sr-Nd) characteristics of Paleoproterozoic anorthositic and granitoid rocks in the Umiakoviarusek Lake region, Labrador, Canada. *Canadian Journal of Earth Sciences* **36**:12, 1957-1972. [Abstract] [PDF] [PDF Plus]
19. James N Connelly, A Bruce Ryan. 1999. Age and tectonic implications of Paleoproterozoic granitoid intrusions within the Nain Province near Nain, Labrador. *Canadian Journal of Earth Sciences* **36**:5, 833-853. [Abstract] [PDF] [PDF Plus]

20. Hamid Telmat, Jean-Claude Mareschal, Clément Gariépy. 1999. The gravity field over the Ungava Bay region from satellite altimetry and new land-based data: implications for the geology of the area. *Canadian Journal of Earth Sciences* **36**:1, 75-89. [Abstract] [PDF] [PDF Plus]
21. Thomas Funck, Keith E. Louden. 1999. Wide-angle seismic transect across the Torngat Orogen, northern Labrador: Evidence for a Proterozoic crustal root. *Journal of Geophysical Research* **104**, 7463. [CrossRef]
22. David J. Scott. 1998. An overview of the UPb geochronology of the Paleoproterozoic Torngat Orogen, Northeastern Canada. *Precambrian Research* **91**, 91-107. [CrossRef]
23. M. J. Van Kranendonk, R. J. Wardle. 1997. Crustal-scale flexural slip folding during late tectonic amplification of an orogenic boundary perturbation in the Paleoproterozoic Torngat Orogen, northeastern Canada. *Canadian Journal of Earth Sciences* **34**:12, 1545-1565. [Abstract] [PDF] [PDF Plus]
24. J. W. F. Ketchum, G. R. Dunning, N. G. Culshaw. 1997. U–Pb geochronologic constraints on Paleoproterozoic orogenesis in the northwestern Makkovik Province, Labrador, Canada. *Canadian Journal of Earth Sciences* **34**:8, 1072-1088. [Abstract] [PDF] [PDF Plus]
25. David J. Scott. 1997. Geology, U – Pb, and Pb – Pb geochronology of the Lake Harbour area, southern Baffin Island: implications for the Paleoproterozoic tectonic evolution of northeastern Laurentia. *Canadian Journal of Earth Sciences* **34**:2, 140-155. [Abstract] [PDF] [PDF Plus]
26. H.A. Wasteneys, S.L. Kamo, D. Moser, T.E. Krogh, C.F. Gower, J.V. Owen. 1997. U#Pb geochronological constraints on the geological evolution of the Pinware terrane and adjacent areas, Grenville Province, southeast Labrador, Canada. *Precambrian Research* **81**, 101-128. [CrossRef]
27. R.J. Thériault, I. Ermanovics. 1997. Sm#Nd isotopic and geochemical characterisation of the Paleoproterozoic Torngat orogen, Labrador, Canada. *Precambrian Research* **81**, 15-35. [CrossRef]
28. Martin J. Van Kranendonk. 1996. Tectonic evolution of the Paleoproterozoic Torngat Orogen: Evidence from pressure-temperature-time-deformation paths in the North River map area, Labrador. *Tectonics* **15**, 843-869. [CrossRef]
29. Derek H.C. Wilton. 1996. Palaeoproterozoic, ~ 1.88–2.0 Ga, organic matter from the Mugford/Kaumajet Mountain Group, northern Labrador. *Precambrian Research* **77**, 131-141. [CrossRef]
30. References 281-318. [CrossRef]
31. David J. Scott. 1995. U–Pb geochronology of a Paleoproterozoic continental magmatic arc on the western margin of the Archean Nain craton, northern Labrador, Canada. *Canadian Journal of Earth Sciences* **32**:11, 1870-1882. [Abstract] [PDF] [PDF Plus]
32. David J. Scott. 1995. U–Pb geochronology of the Nain craton on the eastern margin of the Torngat Orogen, Labrador. *Canadian Journal of Earth Sciences* **32**:11, 1859-1869. [Abstract] [PDF] [PDF Plus]
33. Bruce Ryan. 1995. Morphological features of multigeneration basic dykes near Nain, Labrador: clues to original emplacement mechanisms and subsequent deformation. *Precambrian Research* **75**, 91-118. [CrossRef]
34. Jeremy Hall, Richard J. Wardle, Charles F. Gower, Andrew Kerr, Kevin Coflin, Charlotte E. Keen, Peter Carroll. 1995. Proterozoic orogens of the northeastern Canadian Shield: new information from the Lithoprobe ECSOOT crustal reflection seismic survey. *Canadian Journal of Earth Sciences* **32**:8, 1119-1131. [Abstract] [PDF] [PDF Plus]
35. David J. Scott, Nuno Machado. 1995. UPb geochronology of the northern Torngat Orogen, Labrador, Canada: a record of Palaeoproterozoic magmatism and deformation. *Precambrian Research* **70**, 169-190. [CrossRef]
36. M.J. Van Kranendonk, M.R. St-Onge, J.R. Henderson. 1993. Paleoproterozoic tectonic assembly of Northeast Laurentia through multiple indentations. *Precambrian Research* **63**, 325-347. [CrossRef]
37. Introduction 1-12. [CrossRef]